


RF ENVIRONMENT SIMULATOR



by
Ozan İin


Submitted to Graduate School of Natural and Applied Sciences
in Partial Fulfillment of the Requirements
for the Degree of Master of Science in
Electrical and Electronics Engineering

Yeditepe University
2017

RF ENVIRONMENT SIMULATOR

APPROVED BY:

Prof. Dr. Duygun Erol Barkana
(Thesis Supervisor)



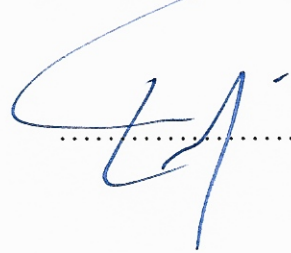
.....

Prof. Dr. Korkut Yeğin



.....

Assist. Prof. Dr. Engin Maşazade



.....

DATE OF APPROVAL:/...../2017

ACKNOWLEDGEMENTS

First of all, I would like to thank to my wife for her endless support and great patience. I would like to express my gratitude towards my family for their encouragement and moral support during the completion of this study.

This thesis would not have been possible without the guidance and support of Professor Korkut Yeğın who has broadened my mind and provided great knowledge during my education.

I am truly grateful to Professor Duygun Erol Barkana who has always willingly helped me and expressed her support.

ABSTRACT

RF ENVIRONMENT SIMULATOR

Evolution of modern communications and radar systems have increased the demand on modelling the propagation effects with real world scenarios for various signal types. The main purpose of this study is to create a flexible, generic and realistic Radio Frequency (RF) environment simulator mainly for radar and communication signals. Software defined radio (SDR) platform has been preferred for generating the simulated signals at radio frequencies. Multipath fading, interference and noise have been calculated for multiple signals simultaneously and generated via RF outputs of the SDR. RF outputs of the proposed configuration are suitable for use in the tests of receivers such as direction finding systems, electronic intelligence, and Long-Term Evolution (LTE) Multiple Inputs Multiple Outputs (MIMO) systems. Communication quality for several signal types has been experimentally investigated with various terrain profiles and fading scenarios using existing vector signal generators, vector signal analyzers, demodulation and communication analysis tools. This simulation platform can be used in Electromagnetic Compatibility tests of such systems as well.

ÖZET

RF ORTAM SİMÜLATÖRÜ

Modern iletişim ve radar sistemlerinin geldiği nokta, RF ortamının etkilerinin çeşitli sinyaller için gerçek dünya senaryolarıyla modellenmesi talebini arttırmıştır. Bu çalışmanın temel amacı hem radar hem de iletişim sinyallerini içeren esnek, genel ve gerçekçi bir radyo frekansı (RF) ortam simülatörü oluşturmaktır. Simülasyonu gerçekleştirilen sinyalleri radyo frekansında üretmek için yazılım tabanlı radyo (SDR) platformu tercih edilmiştir. Çok yollu sönmelenme, girişim ve gürültü birden fazla sayıda sinyal için eş zamanlı olarak hesaplanmış ve SDR'nin RF çıkışları yoluyla üretilmiştir. Sistemin RF çıkışları, yön bulma sistemleri ve LTE MIMO sistemleri gibi alıcıların testlerinde kullanılmaya uygundur. Çeşitli arazi profilleri ve sönmelenme senaryoları için çok sayıda sinyal tipinin iletişim kalitesi, vektör sinyal üreteçlerinden, vektör sinyal analizörlerinden, demodülasyon ve haberleşme analiz araçlarından yararlanılarak incelenmiştir. Bu simülasyon platformu, bu tür sistemlerin Elektromanyetik Uyumluluk testlerinde de kullanılabilir.

TABLE OF CONTENTS

ACKNOWLEDGEMENTS.....	iii
ABSTRACT.....	iv
ÖZET	v
LIST OF FIGURES	viii
LIST OF TABLES.....	xii
LIST OF SYMBOLS/ABBREVIATIONS.....	xiii
1. INTRODUCTION.....	1
2. OUTDOOR CHANNEL MODELLING.....	3
2.1. LARGE SCALE FADING.....	3
2.1.1. Free Space Path Loss	3
2.1.2. Atmospheric Effects	3
2.1.3. Large Scale Fading Models	4
2.2. MULTIPATH PROPAGATION	5
2.3. INTERFERENCE	5
2.4. NOISE	7
2.5. SMALL SCALE FADING	8
2.5.1. Fading Channel Classification.....	9
2.5.2. Statistical Modelling.....	12
2.5.3. Time Variant and Frequency Dependent Phase Reponse.....	15
3. SIMULATION METHODOLOGY	16
3.1. SOFTWARE ARCHITECTURE	16
3.1.1. Frequency Selective Profile.....	18
3.1.2. Power Delay Profile.....	18
3.1.3. Small Scale Fading	21
3.1.4. Time Variant Phase Shift.....	23
3.1.5. Digital Upconversion (DUC).....	24
3.1.6. Interference	25
3.1.7. Noise	27
3.2. HARDWARE ARCHITECTURE	27

3.3. LIMITATIONS	28
4. EXPERIMENTAL INVESTIGATION.....	29
4.1. POWER DELAY PROFILE ON SLOW FADING CHANNEL.....	29
4.1.1. Verification of the Tapped Delay Line Algorithm	29
4.1.2. Error Vector Magnitude (EVM) Measurements	31
4.2. EFFECTS OF TIME DISPERSION	32
4.2.1. Frequency Domain Analysis.....	32
4.2.2. Communication Performance	34
4.3. EFFECTS OF FREQUENCY DISPERSION	36
4.3.1. Frequency Domain Analysis.....	36
4.3.2. Communication Performance	37
4.4. LTE PERFORMANCE.....	41
4.5. INTERFERENCE MEASUREMENTS.....	42
5. CONCLUSIONS	45
REFERENCES	46
APPENDIX A.....	49

LIST OF FIGURES

Figure 2.1. Harmonics and intermodulation products caused by a non linear device in the presence of two tone input.....	7
Figure 2.2. Types of small scale fading [11]	9
Figure 2.3. Relationship between coherence bandwidth and signal bandwidth	10
Figure 2.4. Implementation of Jakes Fading Model.	14
Figure 3.1 Block Diagram of the Channel Emulator Architecture	17
Figure 3.2. Frequency selective profile implementation block diagram	18
Figure 3.3. Tapped Delay Line Algorithm block diagram	19
Figure 3.4. Calculated paths for a sample terrain in Wireless In Site on Terrain Profile Graph	20
Figure 3.5. Calculated paths for a sample terrain in Wireless In Site on Project Window.	21
Figure 3.6. Real part of Jakes fading model output for 8 paths	22
Figure 3.7. Phase response of Jakes fading model output for single path	23
Figure 3.8. Envelope (Magnitude) of Jakes fading model output for single path	23
Figure 3.9. Time varying phase shifts due to reflection coefficients of 8 paths.....	24
Figure 3.10. Three different signals generated from same RF output	25

Figure 3.11. Intermodulation Products	26
Figure 3.12. PXIe-5673e Vector Signal Generator Upconversion Block Diagram.....	28
Figure 3.13. Hardware setup used for experimental investigation	28
Figure 4.1. Amplitude of the pulses at the output of propagation simulation algorithm.....	30
Figure 4.2. Generated signal via VSG for 16-path pulse propagation.....	30
Figure 4.3. Amplitude of the received pulse via VSA.....	30
Figure 4.4. EVM measurements for the 4-QAM signal with 1 M sym/s symbol rate for different maximum delay values.....	31
Figure 4.5. Received spectrum for 1 M sym/s for a 16 QAM signal with 100 ns delay spread and no Doppler shift	32
Figure 4.6. Received spectrum for 1 M sym/s for a 16 QAM signal with 1 us delay spread and no Doppler shift	33
Figure 4.7. Received spectrum for 1 M sym/s for a 16 QAM signal with 4 us delay spread and no Doppler shift	33
Figure 4.8. Constellation plot for 1 M sym/s for a 16 QAM signal with 100 ns delay spread and no Doppler shift	34
Figure 4.9. Constellation plot for 1 M sym/s for a 16 QAM signal with 1 us delay spread and no Doppler shift	35
Figure 4.10. Constellation plot for 1 M sym/s for a 16 QAM signal with 4 us delay spread and no Doppler shift	35

Figure 4.11. Received Spectrum for 10 M sym/s for a 4 QAM signal with 100 ns delay spread and no Doppler shift	36
Figure 4.12. Received Spectrum for 10 M sym/s for a 4 QAM signal with 100 ns delay spread and 1000 Hz Doppler shift.....	37
Figure 4.13. Constellation plot for 1 M sym/s for a 4 QAM signal with 100 ns delay spread and 100 Hz Doppler shift.....	38
Figure 4.14. Constellation plot for 1 M sym/s for a 4 QAM signal with 100 ns delay spread and 1000 Hz Doppler shift.....	39
Figure 4.15. Constellation plot for 10 M sym/s for a 4 QAM signal with 100 ns delay spread and 100 Hz Doppler shift.....	39
Figure 4.16. Constellation plot for 10 M sym/s for a 4 QAM signal with 100 ns delay spread and 1000 Hz Doppler shift.....	40
Figure 4.17. Constellation plot for 100 k sym/s for a 4 QAM signal with 100 ns delay spread and 100 Hz Doppler shift.....	40
Figure 4.18. LTE spectrum for 1 us delay spread and 100 Hz Doppler shift	41
Figure 4.19. LTE spectrum for 100 ns delay spread and 300 Hz Doppler shift.....	41
Figure 4.20. LTE spectrum for 100 ns delay spread and 1000 Hz Doppler shift.....	42
Figure 4.21. VSA spectrum screen for high power adjacent channel signal	43
Figure 4.22. Received spectrum for a 4 QAM and an adjacent pulse.....	43

Figure 4.23. Received spectrum for 1 M sym/s for a 4 QAM signal in the presence of an adjacent pulse..... 44

Figure 4.24. Output spectrum of the non linear function for and 8 PSK and a 16 QAM signal.
..... 44



LIST OF TABLES

Table 4.1. EVM measurements for different delay spread values on a 1 M sym/s 16 QAM signal.....	34
Table 4.2. EVM measurements for different Doppler spread values on a 1 M sym/s 4QAM signal with 100ns delay spread.	38
Table 4.3. EVM measurements on a 4 QAM signal for 100Hz Doppler spread with 100ns delay spread.	38
Table 4.4. EVM measurements for 100Hz Doppler spread with 100ns delay spread.....	42

LIST OF SYMBOLS/ABBREVIATIONS

B_C	Coherence bandwidth
B_D	Doppler bandwidth
B_S	Signal bandwidth
c	Speed of light
d	Distance
f	Frequency
f_c	Carrier frequency
f_d	Doppler frequency
H	Transfer function
K	Rician factor
r	Magnitude of received signal's complex envelope
T_n	Propagation delay on n th path
T_c	Coherence time
T_S	Symbol time
v	Vehicle speed
w_m	Maximum Doppler shift
X_σ	Zero-mean gaussian distributed random variable
λ	Wavelength of an electromagnetic wave
θ_n	Phase shift applied to the signal on n th path
a_n	Attenuation on n th path
σ_t	RMS delay spread
AWGN	Additive white gaussian noise
BW	Bandwidth
CDMA	Code Division Multiple Access
DUC	Digital up converter
EVM	Error Vector Magnitude

Hz	Hertz
IQ	In-phase and Quadrature
ISI	Intersymbol interference
ITU	International Telecommunications Union
km	Kilometer
LTE	Long-Term Evolution
MSym/s	Mega symbol per second
μm	Micro meter
ns	Nano second
NI	National Instruments
NCO	Numerically controlled oscillator
OFDMA	Orthogonal frequency-division multiple access
PL_{dB}	Path loss in decibels
PN	Pseudo-random Noise
PSK	Phase shift keying
QAM	Quadrature Amplitude Modulation
QPSK	Quadrature Phase Shift Keying
RF	Radio Frequency
rms	Root mean square
SDR	Software Defined Radio
T-R	Transmitter-Receiver
VSA	Vector Signal Analyzer
VSG	Vector Signal Generator

1. INTRODUCTION

In the midst of today's very dense electromagnetic environment, increasing data rates and evolving communication technologies has created the necessity for enhanced testing methods of communication systems. Testing the systems and technologies by simulating the propagation of the wireless signals with real hardware has become a crucial need in the assessment of system performance. Whether there is a line-of-sight propagation or not, the signal generated from the transmitter reaches the receiver by being reflected from multiple paths. These reflections are subject to fading, shadowing, time delay, Doppler shift and additional noise due to atmospheric effects, distance, movement of antennas and surrounding objects. Modeling the channels between the transmitters and the receivers on a terrain is the first and most critical stage of simulating an RF environment.

A channel model is the estimation of the change on a propagated signal's amplitude and phase with time and frequency. The methods for modelling and simulating a wireless multipath fading channel was described and well referenced in [1]. Some of the channel functions for time variant linear channels including simulation results were presented in [2]. Simulation of wireless communications has been described and simulation has been executed via MATLAB covering a wide range of parameters effecting the propagation in [3]. Jakes-model has been used in modelling the Doppler spread in a mobile channel [4-5]. Statistical multipath fading models have also been implemented by several companies with various software tools [6-7]

In this study, channel models between transmitter and receiver antennas have been implemented by considering the terrain profile, channel mobility, atmospheric absorption, and selective effects. After the implementation, simulated output of the channel has been generated via a Vector Signal Generator (VSG) to use the system as a channel emulator. Commercial wireless channel emulation systems have already been delivered with many companies with different capabilities [8-10]. Contrary to commercial products, we aim to build a reference system which allows implementation of the channel modelling techniques described in previous and present studies on a software defined radio (SDR). In our proposed system, any signal type and communication technique can be implemented by creating

resultant baseband In-phase and Quadrature (IQ) stream that generates the resultant RF signal within the limitations of selected RF hardware.

Besides channel modeling, RF environment simulation requires modeling the scenario for a terrain in which multiple RF transmitters which can be mounted on different platforms. These multiple transmitters are then subject to different channel models because of the unique geometry and obstacles between the receiver and each transmitter. Interference between the signals from multiple transmitters should also be considered for a more realistic environment model.



2. OUTDOOR CHANNEL MODELLING

2.1. LARGE SCALE FADING

Large-scale fading propagation models are used to predict the mean received signal strength for an arbitrary transmitter-receiver (T-R) separation distance.

2.1.1. Free Space Path Loss

The path between the transmitter and receiver antennas is called line-of-sight when there is no obstruct on it. The free space propagation model can be used in this case by neglecting the reflections from the ground and the objects in the environment [11].

Free-space loss is calculated using the Friis free-space loss equation, which can be expressed as

$$PL_{dB} = -20 \log \left(\frac{\lambda}{4\pi d} \right) \quad (2.1)$$

where λ is the wavelength of the transmitted signal and d is the distance between the transmitter and receiving antennas, both of which are assumed to be omnidirectional.

2.1.2. Atmospheric Effects

Free space propagation model is usually not sufficient for practical channels in which the signal propagates through the atmosphere and near the ground. The first effect is the atmosphere, which is the source of absorption, refraction, scattering and additional noise. Absorption caused by the atmosphere, can be considered as a single attenuation value applied to whole signal over narrow bandwidths. When the BW of the signal is larger, absorption should be modeled by a frequency dependent transfer function [1][12]. This frequency dependent attenuation is mostly caused by atmospheric gases, especially oxygen

and water vapor, as detailedly expressed in [14]. Refraction/reflection is the dominant effect on the signal between 30 MHz and 1 GHz. Attenuation is more significant above 1GHz and refraction/reflection is less influent unless the path is nearly horizontal. Atmospheric multipath also becomes significant above 1GHz and can cause extreme fading on terrestrial microwave links [13]. Atmospheric gases also causes additional noise on the signal which is frequency dependent as well [15]. The momentary atmospheric conditions is also effective both on absorption and noise. Transfer function of the frequency selective atmospheric absorption is given as

$$H(f) = H_0 \exp\{j0.02096f[10^6 + N(f)]l\} \quad (2.2)$$

where $N(f)$ is the complex refractivity of the atmosphere in parts per million [6], [13], [16].

2.1.3. Large Scale Fading Models

Beside the atmospheric effects, geographical features of the terrain between the transmitter and the receiver antennas also results varying attenuation depending on relative positions of the transmitter and the receiver. According to the measurements in the past, mean value of that the path loss $PL(d)$ at a particular location can be modelled as random and log-normally distributed which is dependent on the distance.

$$PL(d)_{dB} = PL(d_0) + 10 \log \left(\frac{d}{d_0} \right) + X_\sigma \quad (2.3)$$

where d_0 is 1 km and X_σ is a zero-mean gaussian distributed random variable (in dB) with standart deviation σ which is often between 6 to 12 dB [11].

However, log-normal distribution is not sufficient to model the propagation accurately on irregular terrains which include highly mountainous profile or many obstacles like trees and buildings. Many propagation models have been developed in the past using the measurements from different terrains. Longley-rice Model [17], Okumura-Hata Model [4] and the International Telecommunications Union (ITU) propagation model [18] are some of

the widely used large scale propagation models used for irregular terrains. The models differentiate on frequency range, complexity, accuracy and terrain profile [13].

2.2. MULTIPATH PROPAGATION

The term multipath fading generally represents the transmission of emitted signal from the transmit antenna to the receive antenna over multiple reflected and/or refracted paths with different amplitudes and phases. Amplitude of the signal in each path has a mean value which is defined by the large scale fading that is mostly used to calculate the slow variations in the signals due to path loss. Since the paths are different in length, signal is subject to different time delay in each path. General representation for a multipath fading channel impulse response is given as

$$h(t, T) = \sum_{n=0}^{N-1} a_n(t) \exp(-j\theta_n) \delta(t - T_n(t)) \quad (2.4)$$

where $a_n(t)$ and $T_n(t)$ represent the attenuation and the propagation delay associated with the n th multipath component respectively, θ_n is the phase shift applied to the signal on n th multipath component and N is the number paths [1], [11].

2.3. INTERFERENCE

One of the major factors that limit the wireless communication performance is interference from other transmitters in the RF environment. If the interference is at the same frequency with the signal of interest, it is called *co-channel interference*. Co-channel interference may be caused by harmonics from a different type of system, unintentional radiators, or signals from a similar system that are some distance away [13]. For instance, in cellular systems, interference between neighbour cells is a performance degrading effect at cell boundaries when same frequency channels are assigned to neighbor cell sites. OFDMA based cellular systems suffer from *inter-cell interference* especially when all frequency channels are fully

reused whereas CDMA systems are more robust to this type of interference as long as their spreading factor is sufficiently large [4].

When the frequency of the interfering signal is not equal to the frequency of the signal of interest but close to it, *adjacent channel interference* occurs. Effect of this type of interference increases especially when the receiver filters are not perfect such that the interfering signal leaks in to the passband or produces third order components. Electromagnetic interactions, or coupling, among RF systems increase when two transmit antennas are nearby each other. This type of electromagnetic interaction is known as *co-site interference*. The interfering signal can either fall into the bandwidth of the wanted signal or if the transmitted power is high, higher order non-linear components may fall in adjacent band and often the signal is not filtered and raises the noise floor to a much wider band. Closely spaced antennas may also suffer from reduced antenna gain and deformed radiation patterns, which limits the overall communication range.

Intermodulation distortion usually occurs when there is co-site interference. Signals coupled into the output stage of a non-linear transmitter can result in intermodulation products the frequencies of which are described by

$$f_{intermodulation} = mf_1 + nf_2 \quad (2.5)$$

where m and n are integers and $(|m| + |n|)$ is the order of the intermodulation product.

Part of the output spectrum of a non-linear device excited by two signals f_1 and f_2 is shown in Figure 2.1 [19].

Intermodulation distortion may also occur at the receiver side mainly in amplifiers and mixers. It is an important parameter for the receivers and it affects the overall performance. Intermodulation products also occur less frequently in passive devices (cables, adapters etc.) such as those found in many transmission systems [20], [21].

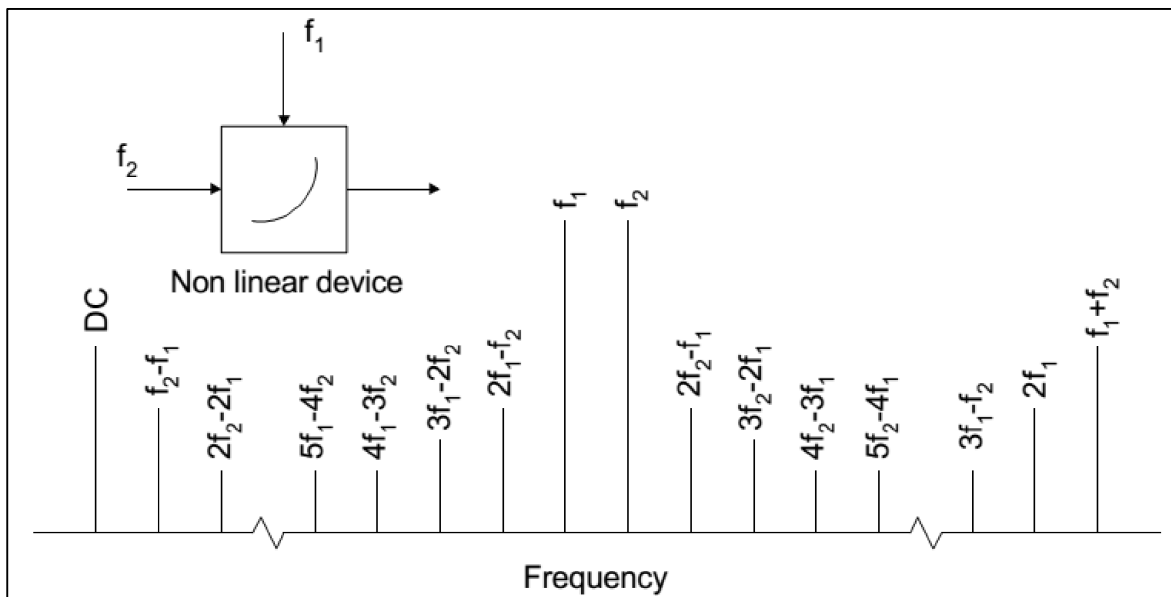


Figure 2.1. Harmonics and intermodulation products caused by a non linear device in the presence of two tone input [19].

Inter-symbol interference (ISI) is another channel effect that can reduce the performance of a digital communication system. The propagation mechanisms that produce ISI are discussed in Chapter 2.5.2.1.

2.4. NOISE

Propagated signal in an RF environment is exposed to external noise which can be attributed to the following causes [15]:

- radiation from lightning discharges (atmospheric noise due to lightning);
- aggregated unintended radiation from electrical machinery, electrical and electronic equipments, power transmission lines, or from internal combustion engine ignition (man-made noise);
- emissions from atmospheric gases and hydrometeors;
- the ground or other obstructions within the antenna beam;

- radiation from celestial radio sources.

Additionally, thermal noise generated in the internal components of RF transmitters should be taken in to account when estimating the overall noise. Another noise effect is caused by interference discussed in the previous Chapter.

2.5. SMALL SCALE FADING

Small Scale Fading or Multipath Fading describes the rapid changes in channel conditions and the resulting changes in the received signal characteristics in mobile communications. The reasons for small scale fading are usually atmospheric conditions or relative motion of the transmitting and receiving antennas, as is the case in mobile communications. Small Scale Fading describes the random fluctuations in the received signals amplitude and phase on the order of a wavelength. The two main sources of this time varying nature of a channel are:

- The relative motion between the transmitter and receiver results in random frequency modulation due to different Doppler shifts on each of the multipath components.
- If objects in the radio channel are in motion, they induce a time varying Doppler shift on multipath components. If the surrounding objects move at a greater rate than the mobile, then this effect dominates fading [22].

Accordingly, channel can be degraded to a time varying impulse response and can be expressed as

$$h(t, T) = \sum_{n=0}^{N-1} a_n(t) e^{-j(2\pi f_c T_n(t) + \varphi_n(t))} \delta(t - T_n(t)) \quad (2.6)$$

where the phase term, $2\pi f_c T_n(t) + \varphi_n(t)$, represents the phase shift due to the delay caused by the path-length differences and the additional phase shifts encountered on the path [1].

2.5.1. Fading Channel Classification

Small Scale Fading channels are classified based on Doppler spread and based on multipath time delay spread as described in Figure 2.2.

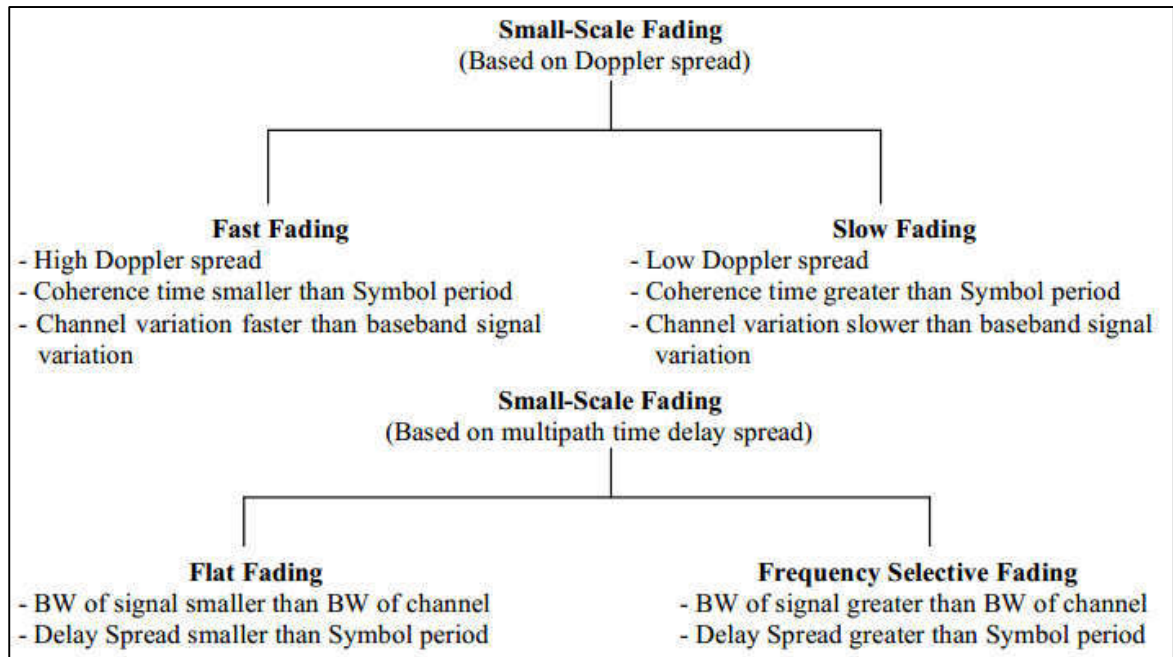


Figure 2.2. Types of small scale fading [11].

2.5.1.1. Time Spreading

A mobile radio channel has a *coherence bandwidth* over which gain is almost constant and phase is linear (Fig. 2.3) [3]. Roughly, if the bandwidth of the transmitted signal is smaller than the channel bandwidth the signal is subject to flat fading. If the bandwidth of the transmitted signal is larger than the channel bandwidth the signal is subject to frequency selective fading. Time dispersion of the channel is caused by multipath fading and when analyzed in time domain, coherence bandwidth of the channel is determined by root mean square (rms) delay spread of multipath components [22]. The coherence bandwidth is often approximated as

$$B_c \approx \frac{1}{5\sigma_t} \text{ to } \frac{1}{50\sigma_t} \quad (2.7)$$

where B_c is the coherence bandwidth of the channel and σ_t is rms delay spread.

In summary, flat fading is present if

$$B_s \ll B_c \quad (2.8)$$

and

$$T_s \gg \sigma_t \quad (2.9)$$

where B_s is the signal bandwidth and T_s is the symbol duration.

Frequency selective fading is present if

$$B_s > B_c \quad (2.10)$$

and

$$T_s < \sigma_t. \quad (2.11)$$

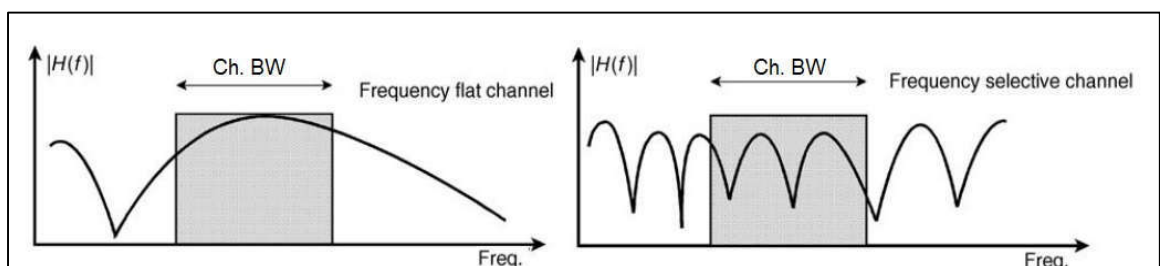


Figure 2.3. Relationship between coherence bandwidth and signal bandwidth [3].

When the delay spread is of the order of, or greater than, the symbol duration in a digital communication system, the delayed multipath components will arrive in different symbol intervals and cause inter-symbol interference, which can adversely impact the BER performance [1].

2.5.1.2. Frequency Spreading

Another important parameter of a mobile channel, *coherence time*, is defined as the time duration over which the signal amplitude will be highly correlated (close to constant). In other words coherence time is a measure of how rapidly does channel impulse response change. The channel is called slow fading channel if the coherence time is much larger than the symbol duration. If the coherence time is smaller than symbol duration, than the channel is called as fast fading channel.

Frequency spreading of the channel is related to the relative motion in the channel which results both positive and negative Doppler shift on the signal. This effect is called in Doppler spread and modeling the Doppler spread is discussed in Section 2.5.2.3. The coherence time is often approximated as

$$T_c \approx \frac{1}{B_D} \quad (2.12)$$

where T_c is the coherence time of the channel and B_D is Doppler spread which is equal to maximum Doppler shift in the channel.

In summary, slow fading is present if

$$T_S \ll T_c \quad (2.13)$$

and

$$B_S \gg B_D \quad (2.14)$$

where B_S is the signal bandwidth and T_S is the symbol duration.

In summary, fast fading is present if

$$T_S > T_C \quad (2.15)$$

and

$$B_S < B_D. \quad (2.16)$$

2.5.2. Statistical Modelling

Small-scale fading is generally characterized by a Rayleigh or Rician probability in mobile radio channels.

2.5.2.1. Rayleigh Fading

When communications occur in a multi-path environment without LOS, the amplitude of the received signal has typically a Rayleigh distribution. Rayleigh fading model assumes that the magnitude of a signal that has passed through transmission medium will vary randomly according to a Rayleigh distribution. Rayleigh fading is a reasonable model when there are many objects in the environment that scatter the radio signal before it arrives at the receiver. Rayleigh fading is most applicable when there is no dominant line-of-sight propagation between the transmitter and receiver. Phases of the paths are assumed to be uniformly distributed in $(0, 2\pi)$, and the distribution is expressed as:

$$f(r) = \frac{r}{\sigma^2} \exp\left(-\frac{r^2}{2\sigma^2}\right) \quad \text{for } r \geq 0 \quad (2.17)$$

where r is the magnitude of the received signal's complex envelope and σ^2 is the variance of the real and imaginary parts [3].

2.5.2.2. Rician Fading

An alternative channel model can be obtained when one major strong fixed path (usually line-of-sight) with a known magnitude is present in addition to the N weaker paths. In this case the received signal can be formulated as

$$R(t)e^{j\theta(t)} = u(t)e^{j\alpha(t)} + A(t)e^{j\beta(t)} \quad (2.18)$$

where $u(t)$ is Rayleigh distributed, $\alpha(t)$ is uniform in $(0, 2\pi)$ and $A(t)e^{j\beta(t)}$ is the deterministic (line-of-sight) signal. Eventually, the envelope $R(t)$ has Rician distribution expressed as

$$f(r) = \frac{r}{\sigma^2} \exp\left(-\frac{r^2 + A^2}{2\sigma^2}\right) I_0\left(\frac{Ar}{\sigma^2}\right) \quad \text{for } A \geq 0 \text{ and } r \geq 0 \quad (2.19)$$

where A is the peak amplitude of the direct component and I_0 denotes the zeroth-order modified Bessel function. As a result $R(t)$ and $\theta(t)$ are independent processes where $\theta(t)$ is uniform in $(0, 2\pi)$ [1].

2.5.2.3. Jakes Model

The Jakes fading model is a deterministic method for simulating time-correlated Rayleigh fading waveforms and is still widely used today. The model assumes that N equal-strength rays arrive at a moving receiver with uniformly distributed arrival angles $\alpha(t)$, such that ray “ n ” experiences a Doppler shift $w_{n=} w_m \cos(\alpha_n)$ where $w_m = 2\pi f v/c$ is the maximum

Doppler shift, v is the vehicle speed, f is the carrier frequency and c is the speed of light [5]. The Jakes fading model provides multiple time correlated fading waveforms, but the waveforms are not truly uncorrelated with one another. The model has been reformulated in [5] with different ray arrival angles such that N_0 uncorrelated fading waveforms are generated.

The function which generates the j th waveform after the modification is

$$C(t, j) = \sqrt{\frac{2}{N_0}} \sum_{n=1}^{N_0} A_j(n) \{ [\cos(\beta_n) + I \sin(\beta_n)] \cos(w_n t + \theta_n) \} \quad (2.20)$$

where $A_j(n)$ is the j th Walsh-Hadamard (WH) codewords and $\beta_n = \pi n / N_0$.

Implementation of Jakes Model has been shown in [4], and reproduced in Figure 2.4.

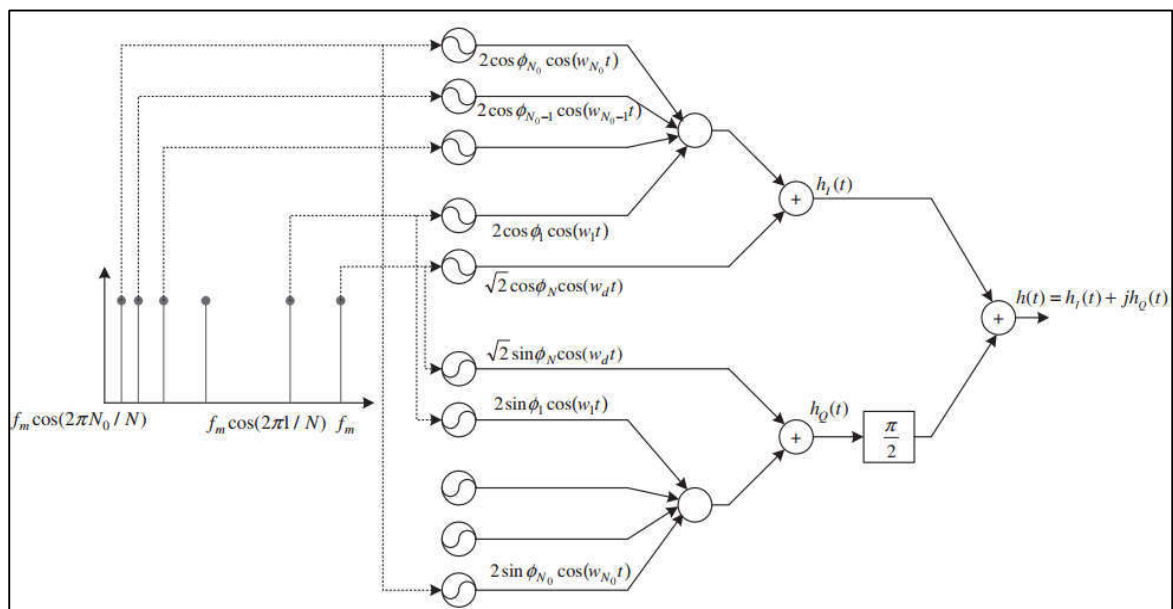


Figure 2.4. Implementation of Jakes Fading Model [4].

The multiple components with different Doppler shifts causes the transmitted signal to spread in frequency (Doppler Spread). The effect in the frequency domain can be expressed with a power spectral density which is given as

$$S_d(f) = \begin{cases} \frac{K}{\sqrt{1 - (f/f_d)^2}}, & |f| < f_d \\ 0, & \text{otherwise} \end{cases} \quad (2.21)$$

where f_d is the maximum Doppler shift.

Jakes Doppler spectrum can also be implemented with a filter whose transfer function is

$$H(f) = \begin{cases} [1 - (f/f_d)^2]^{-1/4}, & |f| < f_d \\ 0, & \text{otherwise} \end{cases} \quad (2.22)$$

2.5.3. Time Variant and Frequency Dependent Phase Response

Reflection coefficient, another important factor on propagation, is a complex parameter where both phase and amplitude of the coefficient are dependent on frequency, grazing angle, material properties and polarization. As a result, each path has different frequency response of amplitude and phase [13]. The effects of the atmospheric absorption and the reflection coefficient can be modelled as a filter with nonlinear phase response when they are considered together.

On the other hand, the channel geometry changes in time when there is a motion in the channel. This time variant nature results in variable reflection and diffraction points for the paths which means possibly different phase of reflection coefficient at particular periods. This behavior, which is included in the simulations of this study, is usually neglected in channel modelling studies.

3. SIMULATION METHODOLOGY

Simulations have been executed utilizing a software defined radio (SDR) architecture which includes both software and hardware components.

3.1. SOFTWARE ARCHITECTURE

NI LabVIEW has been used for implementing the wireless channel model algorithm and creating relevant complex baseband signal. This section describes the steps implemented for simulating the propagation channel. Since the algorithms are applied to a real world signal which is generated via an RF generator as displayed in Figure 3.1, this study can be referred as channel emulation or RF environment emulation. Flexible and scalable architecture of the selected hardware allows the implemented software to be used with multiple devices to test MIMO techniques, interference tests.

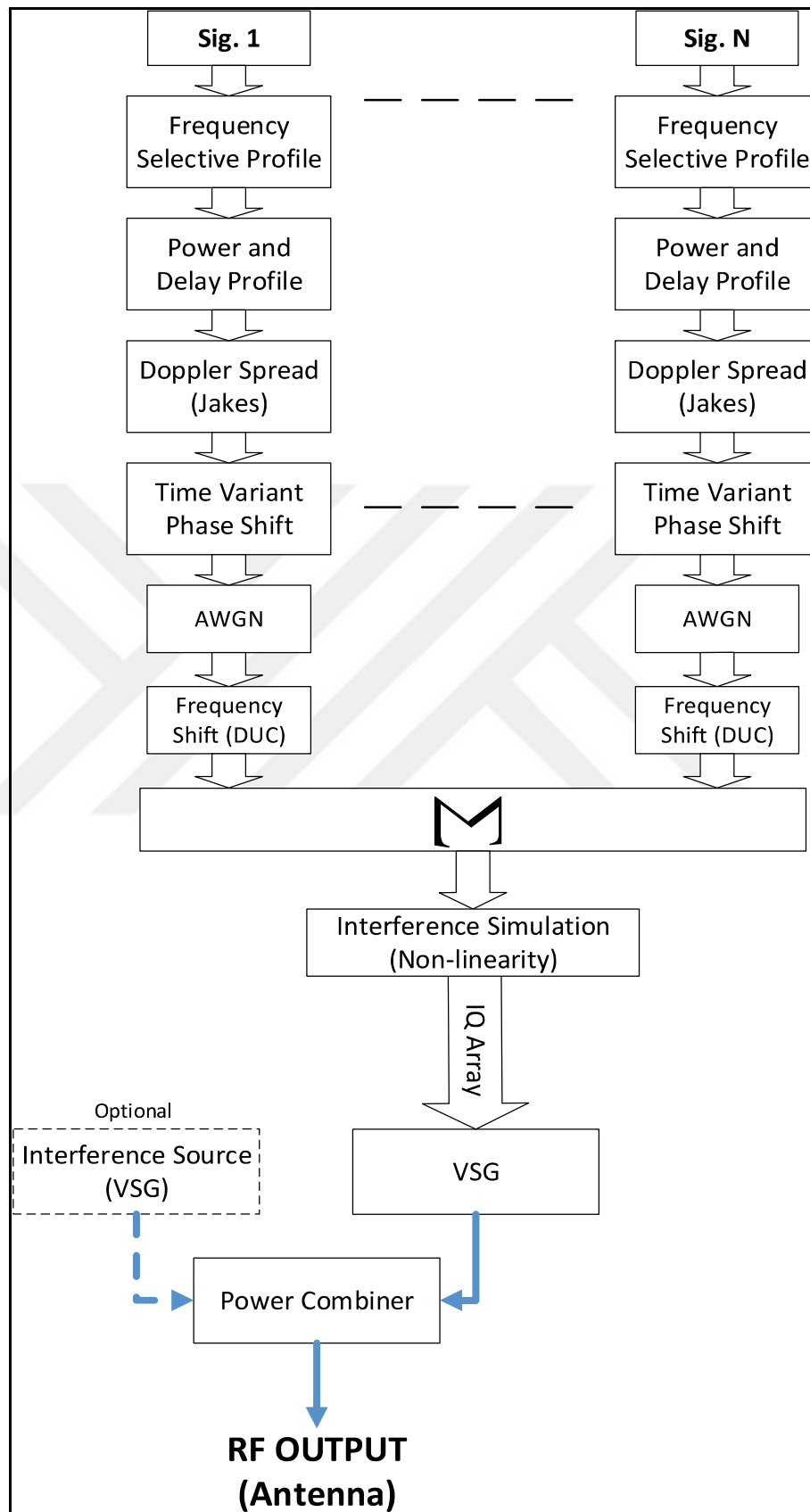


Figure 3.1. Block diagram of the Channel Emulator Architecture.

3.1.1. Frequency Selective Profile

As discussed in Sections 2.1.2 and 2.5.3, amplitude and phase responses of a propagation path are dependent on frequency. A frequency domain filter with non-linear phase response has been implemented for this purpose. Atmospheric effects does not change significantly between multiple paths. However, reflection coefficients may vary significantly between paths which results in different amplitude and phase responses on frequency domain. After a common frequency response has been determined for all the paths, the filter response should be modified for each path considering different reflection geometry. It has been preferred to create the filter response in the frequency response since the measurements from previous research are usually given in frequency domain. Inverse Fast Fourier Transform has been used to observe the filter transfer function which has been convolved with the input signal as shown in Figure 3.2.

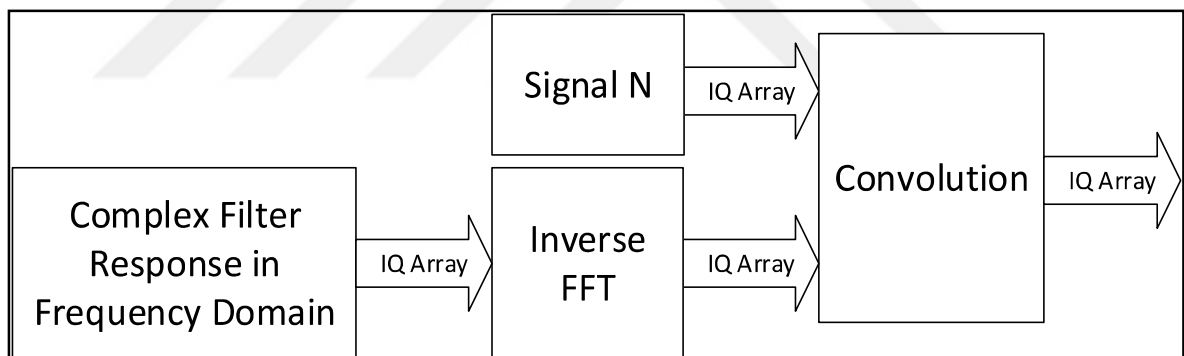


Figure 3.2. Frequency selective profile implementation block diagram.

3.1.2. Power Delay Profile

The second step in simulating the channel is calculating the power-delay profile (long term values of a_n and T_n) for the selected terrain. The profile has been calculated in LabVIEW first in order to analyze the effects of time spreading of the channel with controlled delay spread values. Log normal distribution given in (2.3) has been used to calculate received power a_0 for the mean distance d which gives T mean delay value with the assumption $X_\sigma =$

0. a_n and T_n are then calculated for each path assuming that both of them are and gaussian distributed random variables (in dB) around a_0 and T_0 respectively.

Tapped Delay Line Algorithm has been used to implement power-delay profile. In order to apply the desired delay values to input signal, required number of zeros has been inserted to the beginning of the complex input array which carries the signal information.

$$m = \frac{T_n}{T_s} \quad (3.1)$$

where m_n is the number of zeros inserted and T_n is the required delay for the nth path, T_s is the sampling interval as illustrated in Figure 3.3.

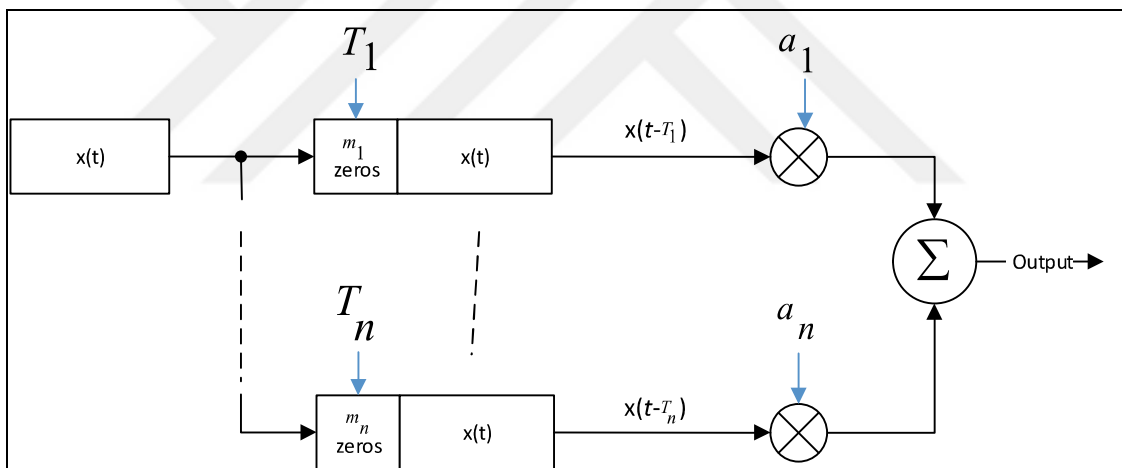


Figure 3.3. Tapped Delay Line Algorithm block diagram.

In order to simulate the large scale fading more accurately, Wireless In-Site software by REMCOM [23] has been used for power-delay profile which can be calculated using the geographical properties of selected terrain between the transmitter and the receiver antennas. Wireless InSite is an electromagnetic simulation tool for predicting the effects of buildings and terrain properties on the propagation of electromagnetic waves. It predicts how the locations of the transmitters and receivers within an urban area affect signal strength. Wireless InSite, models the physical characteristics of irregular terrain and urban building features, performs the electromagnetic calculations, and then evaluates the signal

propagation characteristics. The calculations are made by shooting rays from the transmitters and propagating them through the defined geometry. These rays interact with geometrical features and make their way to receiver locations. Ray interactions include *reflections* from feature faces, *diffractions* around feature edges, and *transmissions* through features faces. Wireless InSite's ray-based solvers use the Uniform Theory of Diffraction (UTD) to evaluate a ray path's electric field. UTD provides accurate results when the scenario geometry is large compared to the wavelength of the propagating wave. For typical applications, the UTD-based models provide accurate predictions from approximately 100 MHz to approximately 100 GHz [24]. The output of the calculations is given as a time invariant $3 \times N$ matrix which includes attenuation, delay and the arrival angle for N paths as displayed in Figures 3.4 and 3.5.

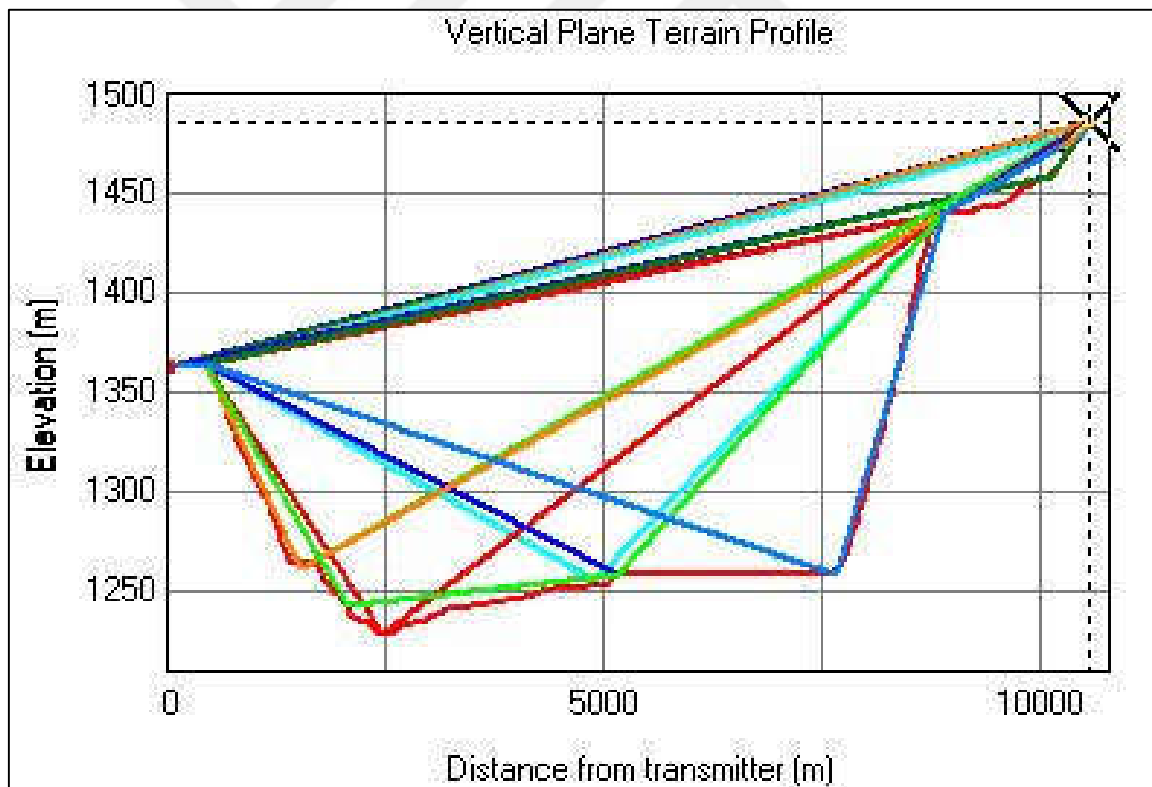


Figure 3.4. Calculated paths for a sample terrain in Wireless In Site on Terrain Profile.

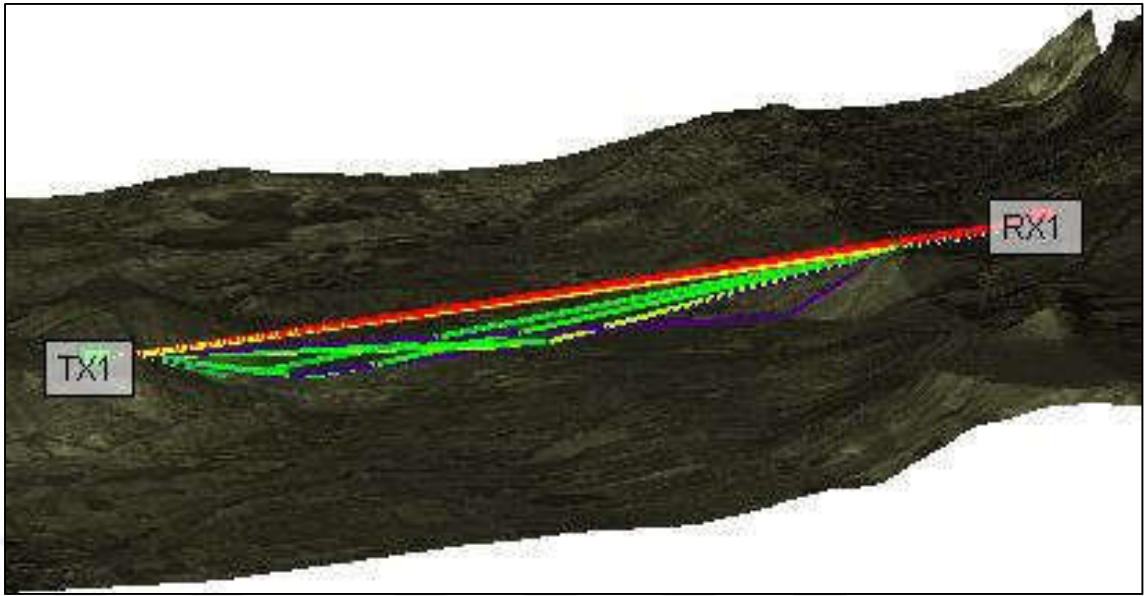


Figure 3.5. Calculated paths for a sample terrain in Wireless In Site on Project Window.

3.1.3. Small Scale Fading

Jakes mobile channel model which is a deterministic model for generating Rayleigh distributed fading is used to generate Doppler filtered small scale envelope of each path. In Jakes model, a large number of sinusoids are added in order to produce approximate Rayleigh amplitude. The function that is used to produce Jakes Doppler spectrum was formed based on the revision to Jakes Model proposed in [5]. For an 8-path simulation model, outputs off Jakes fading model are displayed in Figure 3.6. Phase and magnitude responses for a single ray are shown in Figures 3.7 and 3.8.

When power-delay profile includes a specular component, Rician model can be obtained from the Rayleigh model by adding a nonzero mean [1]. The ratio of power of specular component to the power of random component is called Rician K factor and it is defined as

$$K = \frac{A^2}{\sigma^2}. \quad (3.2)$$

To simulate a Rician Fading channel, mean and sigma has to be calculated with the given Rician K factor.

If mean (m) and sigma (σ) are defined as

$$m = \sqrt{\frac{K}{K+1}} \quad (3.3)$$

$$\sigma = \sqrt{\frac{1}{2(K+1)}} \quad (3.4)$$

then, the received signal can be expressed as

$$R(t)e^{j\theta(t)} = mu_0(t)e^{j\alpha_0(t)} + \sigma \sum_{n=1}^{N-1} u_n(t)e^{j\alpha_n(t)} \quad (3.5)$$

where mu_0 and α_0 are the amplitude and phase of the LOS component, respectively, and σu_n and α_n are the amplitude and phase of the n th multipath scattered component, respectively. “MT Rician Fading Profile” and “MT Rayleigh Fading Profile” functions have been used in LabVIEW Modulation toolkit which generates the profiles explained in this Chapter.

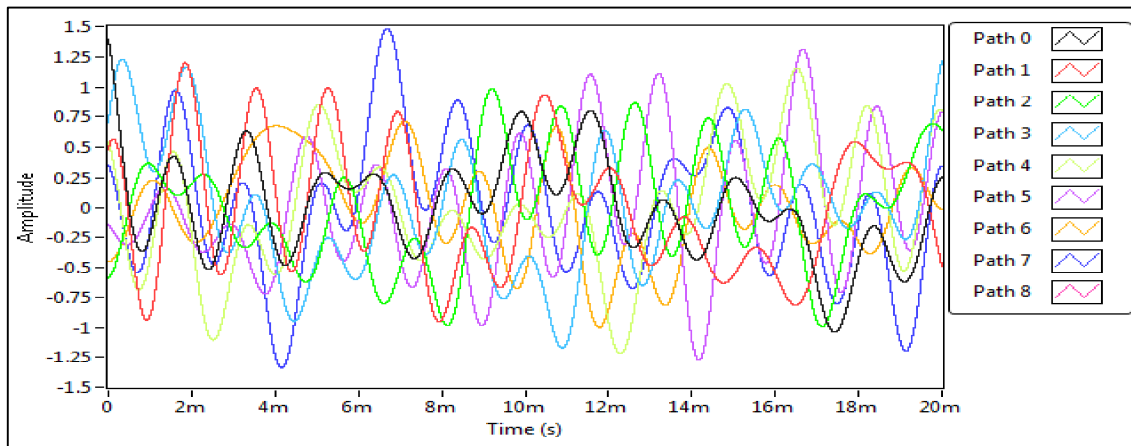


Figure 3.6. Real part of Jakes fading model output for 8 paths.

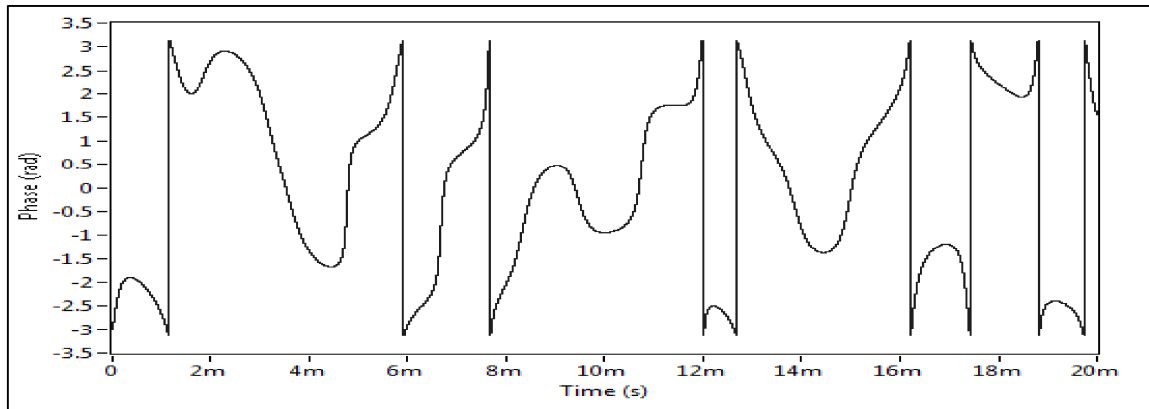


Figure 3.7. Phase response of Jakes fading model output for single path.

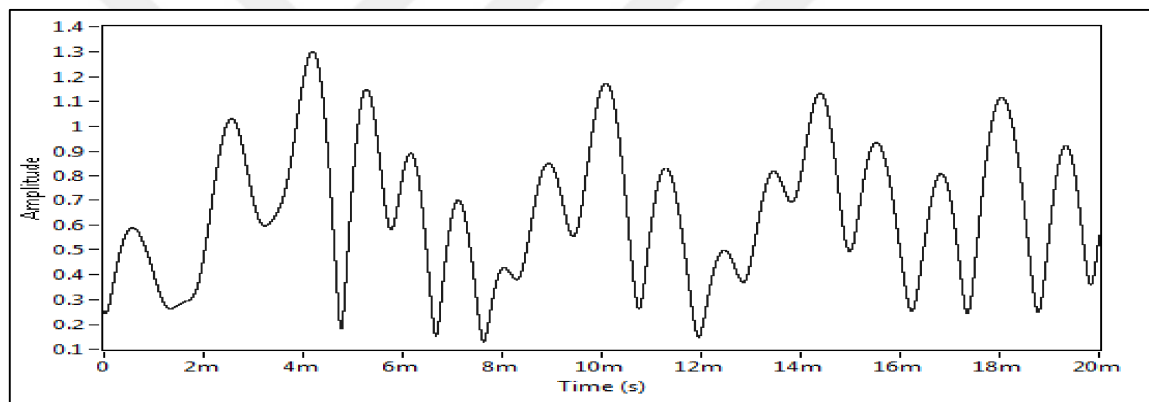


Figure 3.8. Envelope (Magnitude) of Jakes fading model output for single path.

3.1.4. Time Variant Phase Shift

Jakes fading model does not encounter the rapid phase changes in a mobile channel due to the time varying geometry between the transmitter and the receiver antennas. As the reflection surface changes from a building to a rough surface or from water to a metallic obstacle etc., the phase shift applied to the signal because of the reflection may change significantly. Time varying phase shift due to reflection coefficient is dependent on the grazing angle and the material properties and should be considered while calculating $\varphi_n(t)$ in (2.6). In this context, a continuous time variant phase response must be defined in order to properly simulate phase variations and discontinuities in a mobile channel. Time varying phase shifts implemented on 8-path simulation are shown in Figure 3.9.

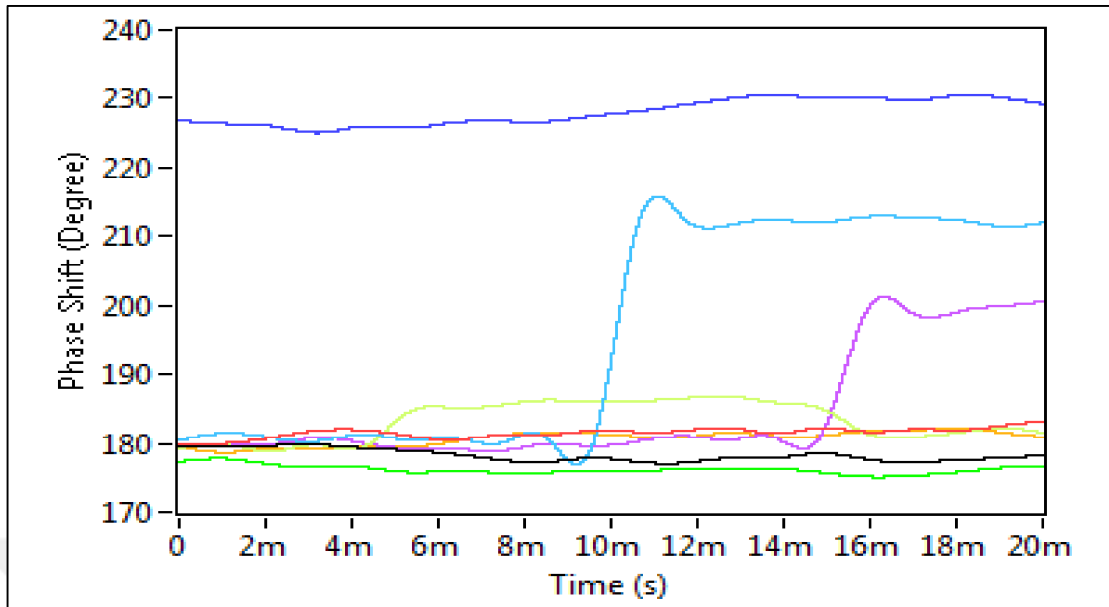


Figure 3.9. Time varying phase shifts due to reflection coefficients of 8 paths.

3.1.5. Digital Upconversion (DUC)

One of the main objectives of RF Environment Simulation is that multiple signals with adjustable frequency offsets with independent bandwidths and channel models can be generated simultaneously as in Figure 3.1. The frequency shifting operation has been implemented via Digital Upconversion (DUC) algorithm. The DUC algorithm passes the baseband complex signal from a complex mixer which multiplies the input signal with complex NCO.

If the the baseband output of the channel model is represented as a complex array $x = x_r + x_i$ then, the NCO signal becomes a complex array $n = n_r + n_i$. Output can be calculated as $= xn = y_r + y_i$. Direct implementation requires four real multiplications:

$$y_r = x_r n_r - x_i n_i \quad (3.6)$$

$$y_i = x_r n_i + x_i n_r \quad (3.7)$$

Three different signals generated at the same RF output is illustrated in Figure 3.10.

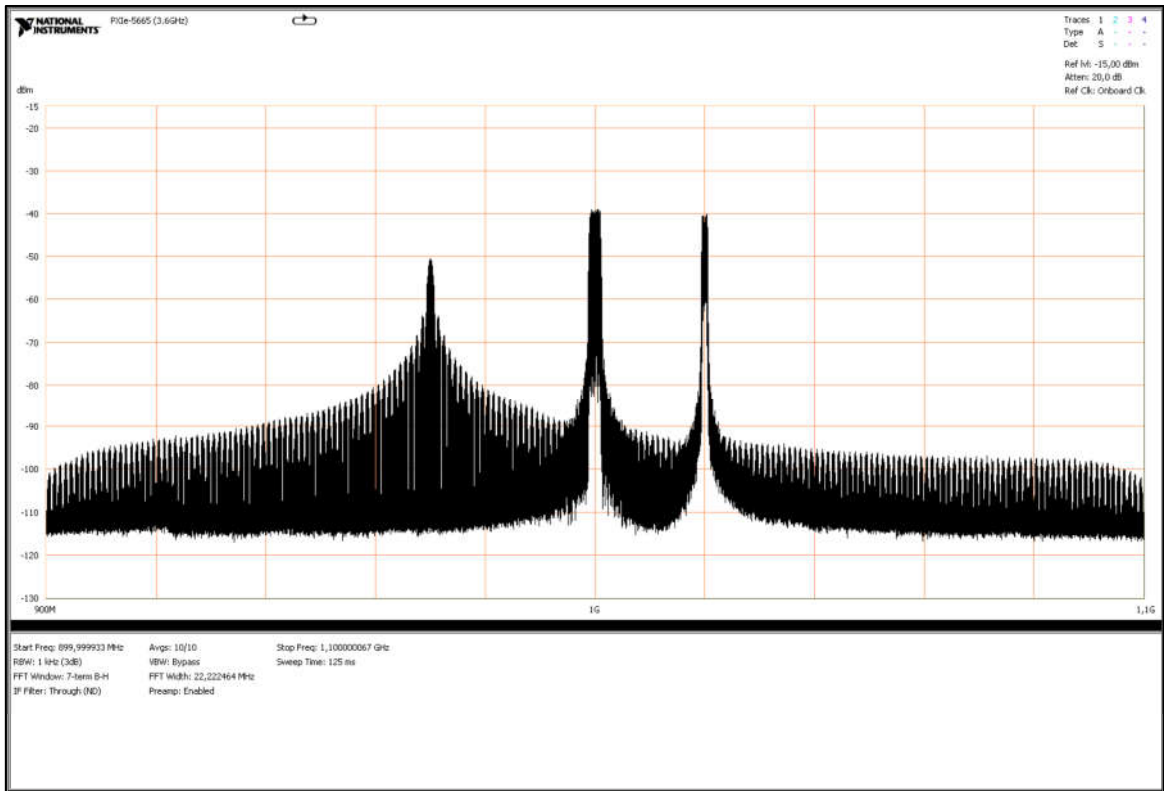


Figure 3.10. Three different signals generated from the same RF output.

3.1.6. Interference

Interference can be of such a nature that it appears to be externally generated noise. This is often how interference analysis is performed most of the time, however, interference is not noise-like, which makes precise performance analysis difficult [13]. In this study inference simulation has been implemented in a more realistic way. Different types of interferences has been simulated with the help of DUC architecture and an additional RF Signal Generator.

A nonlinear system model function has been used to generate the harmonics and intermodulation products as if it is generated by one of the multiple transmitters or by passive components. The function is expressed as

$$y = x(1 - d_1(d_1x + d_2x^2 + d_3x^3 + d_4x^4 + d_5x^5)) \quad (3.8)$$

Where x is the input signal, d_1, \dots, d_5 are distortion coefficients. Output spectrum of this function has been generated in LabVIEW as can be seen in Figure 3.11 when two tones are applied to its inputs.

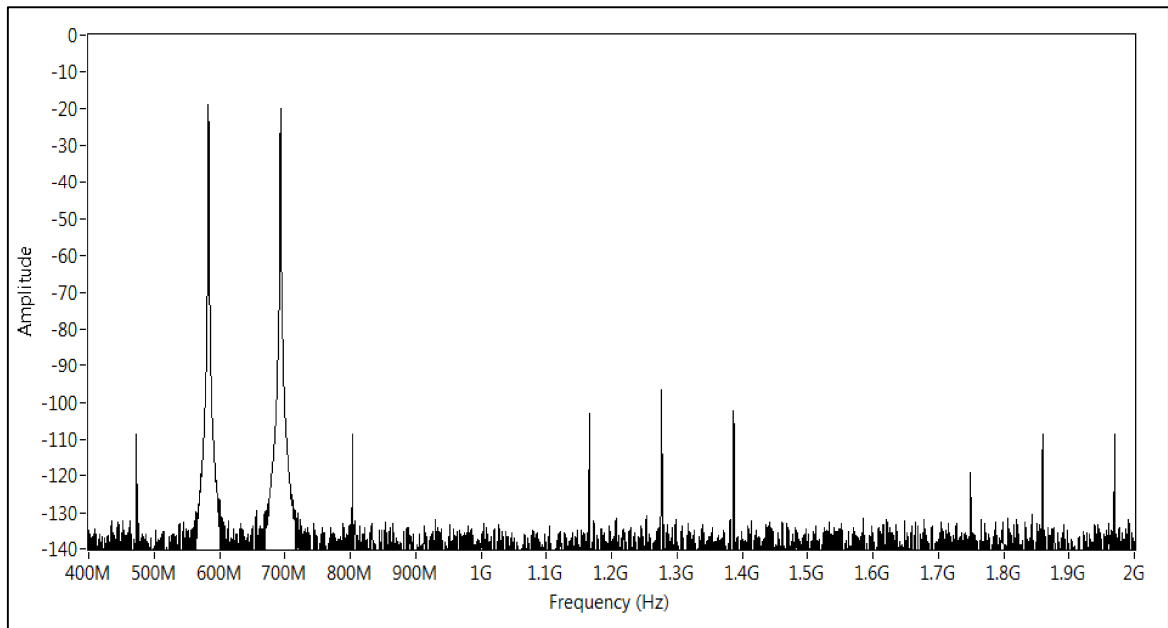


Figure 3.11. Intermodulation products

These third order components are used as interference and distortion sources for the signals at different frequencies. For instance, one of the intermodulation products can be considered as co-channel interference or external noise when it is at the same frequency with the signal of interest. Co-site interference is caused when a friendly transmitter is co-located or nearby located to the receiver antennas. If the power transmitted is high, higher order non-linear components may fall in adjacent band and often the signal is not filtered and raises the noise floor of a much wider band. This can be simulated as well with the nonlinear system function which can be considered as the effect of 3rd-order intermodulation products of the power amplifier.

Adjacent channel interference is simulated by generating an RF pulse in the adjacent band. The amount of interference can be controlled by varying the pulse width and transmitted power. A communication signal can also be used as adjacent channel interference source when its frequency is close to another signal.

Multiple VSGs can be used for separating the channel models of the emitters to increase the dynamic range and creating non-linear effects produced by RF components. When a strong signal is generated at the adjacent signal band with the signal of interest, non-linear effects can be observed in the band-of interest.

3.1.7. Noise

In addition to the noise effect caused by the interference, additive white Gaussian noise (AWGN) also has been generated in order to simulate overall noise effect in the RF environment. Since noise caused by transmitters and antennas should be simulated as well, every signal has been exposed to different noise levels when multiple signals are generated with independent channel models.

3.2. HARDWARE ARCHITECTURE

The SDR platform selected for communication performance tests is composed of two separate hardware components as vector signal generator (VSG) and vector signal analyzer (VSA). The term “vector” emphasizes complex signals which allow manipulating and interpreting the phase and the magnitude of the signal.

Complex baseband output of the channel model algorithm has been transferred to onboard memory of the arbitrary waveform generator which is a part of the VSG. VSG upconverts the baseband signal to any center frequency between 85 MHz and 6.6 GHz as seen in Figure 3.12. Generated RF signal has been received via an RF cable and converted to complex baseband IQ by NI PXIe-5665 vector signal analyzer for performance tests. Hardware setup is displayed in Figure 3.13. The power combiner has been used to combine the outputs of VSG and the interference generator.

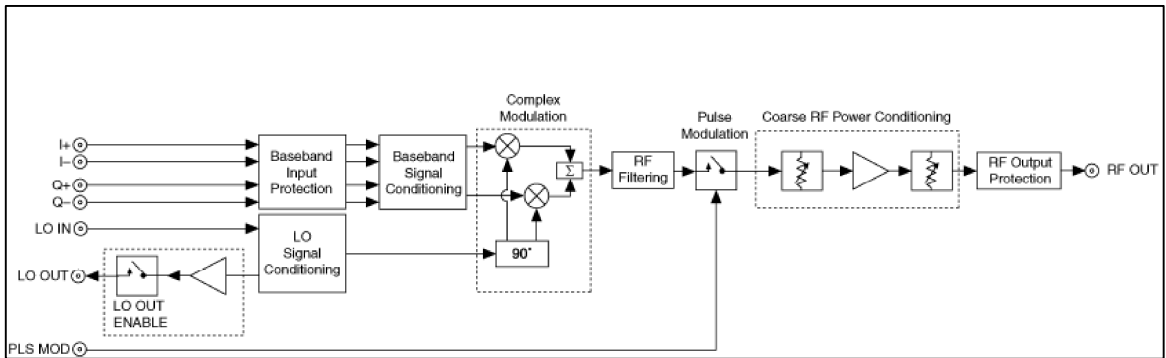


Figure 3.12. PXIe-5673e Vector Signal Generator Upconversion Block Diagram.

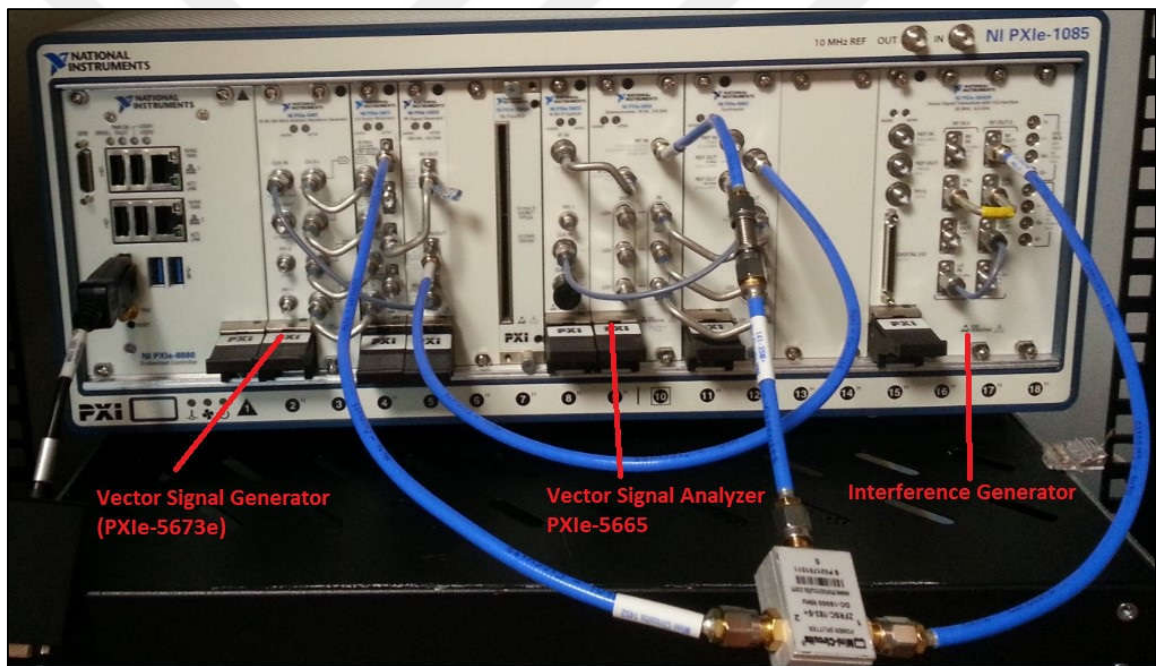


Figure 3.13. Hardware setup used for experimental investigation.

3.3. LIMITATIONS

Although SDR platforms reduce the effort to build prototype systems with their programmability, they also bring some hardware limitations. The analog bandwidth of NI PXIe-5673e which is about 110 MHz restricts the frequency offset between multiple signals. Overall spurious free dynamic range is not better than 80 dB and the overall operating frequency range which is between 85 MHz and 3.6 GHz.

4. EXPERIMENTAL INVESTIGATION

The measurements to analyze different effects of RF environment are explained in detail in this chapter. All measurements have been realized with real hardware as shown in Figure 3.13.

4.1. POWER DELAY PROFILE ON SLOW FADING CHANNEL

Generation and implementation of power-delay profile has been the first step of simulation tests. Communication performance for different delay spread values have been measured after the verification of the algorithm.

4.1.1. Verification of the Tapped Delay Line Algorithm

As the first step of measurements, implemented tapped delay line algorithm has been verified via transmitting an RF pulse with 1 microsecond (μs) pulse width and 400 nanosecond (ns) excess delay. 16-path propagation has been simulated on the computer first, and the propagated pulses from 16 paths were consistent with the predefined power and delay profile. The baseband pulse has then been upconverted via the VSG and received by the VSA. Shape of received pulse matched to the simulation except some little distortion on the signal due to the lower sampling rate of the VSA and some additional noise caused by the hardware as displayed in Figures 4.1, 4.2, and 4.3.

The time axis of Figure 4.3. is different than Figure 4.2. since the generator and the analyzer have independent clocks and there is no triggering mechanism between them. However, it can be observed that the pulse width of the signal is almost the same with the simulation at every amplitude point.

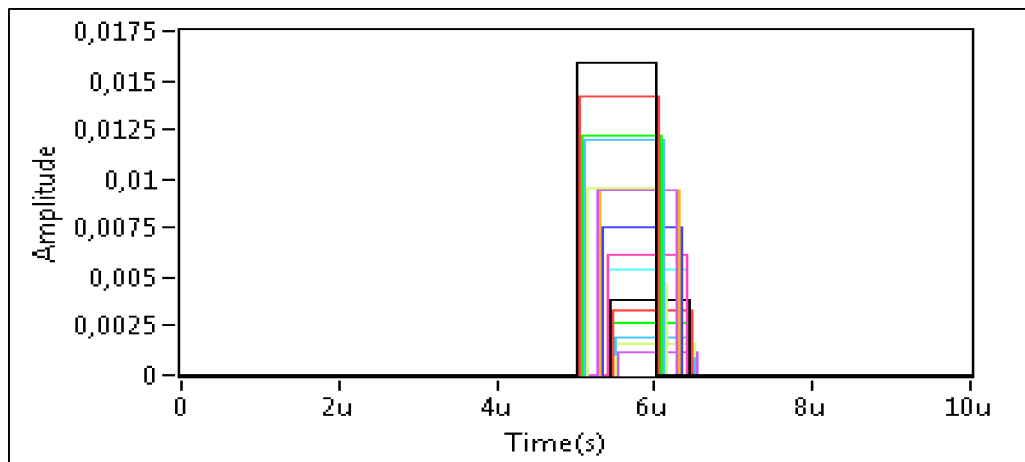


Figure 4.1. Amplitude of the pulses at the output of propagation simulation algorithm.

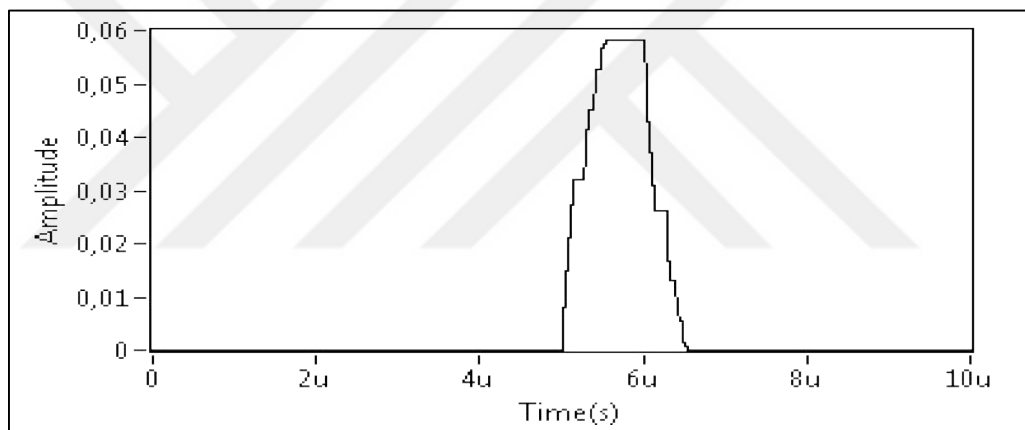


Figure 4.2. Generated signal via VSG for 16-path pulse propagation.

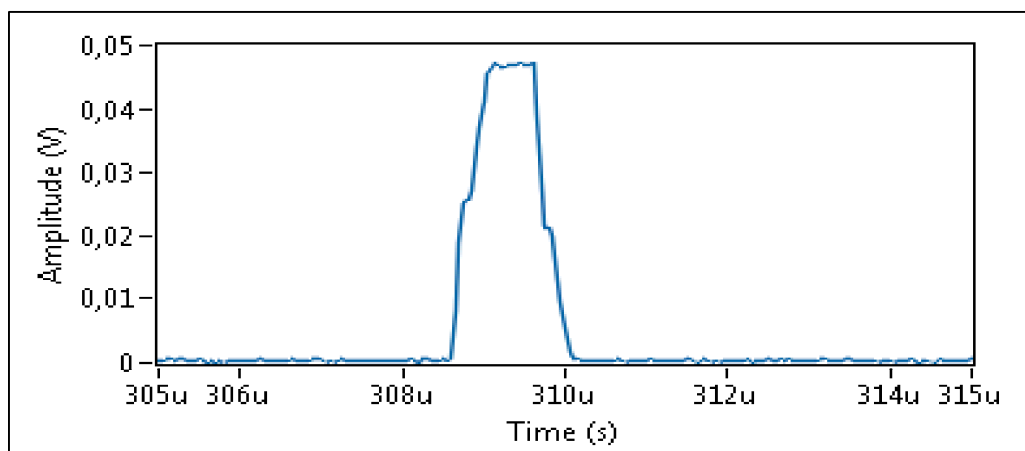


Figure 4.3. Amplitude of the received pulse via VSA

4.1.2. Error Vector Magnitude (EVM) Measurements

Before using power-delay profile from Wireless In Site, the power-delay profiles calculated in LabVIEW have been used to analyze the impact of various path number, attenuation and delay values on communication performance. 4-Quadrature Amplitude Modulation (QAM) signal has been generated for this purpose and the received signal has been demodulated. EVM values have been measured for original signal and various delay spread and additional noise values. The EVM measurements for the 4-QAM signal for different power-delay profiles are shown in Figure 4.4. It is observed that demodulation accuracy is degraded even when the coherence bandwidth (BW) of the channel is higher than the signal BW.

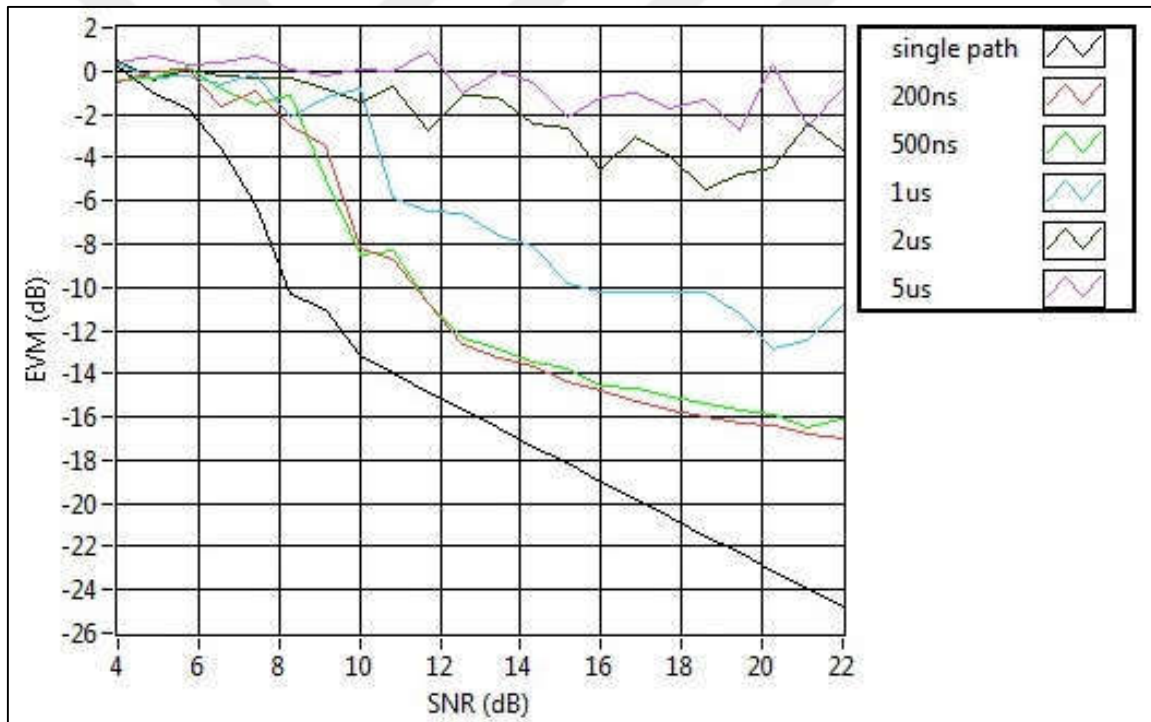


Figure 4.4. EVM measurements for the 4-QAM signal with 1 M Sym/s symbol rate for different maximum delay values.

4.2. EFFECTS OF TIME DISPERSION

Effects of time dispersion have been investigated first on frequency domain in order to see the filter effect of the channel. After that, communication performance has been investigated with communication analysis tools.

4.2.1. Frequency Domain Analysis

Coherence BW of a propagation channel is inversely proportional to delay spread. Hereby, a filter effect should be observed at the output of the FFT function which transforms the time domain signal to frequency domain. A 16 QAM Pseudo-random Noise (PN) sequence has been used as the transmitted signal and resultant spectrum graphs are shared. In Figure 4.5, the signal is totally in the passband of the channel filter and there is no significant attenuation on the edges of signal's spectrum. This result corroborates expectations since the bandwidth of the channel is greater than 2MHz when the delay spread is 100 ns. The channel starts to filter the signal significantly as the delay spread increases. Increase in the delay spread decreases the channel bandwidth where the signal bandwidth remains unchanged as illustrated Figures 4.6 and 4.7.

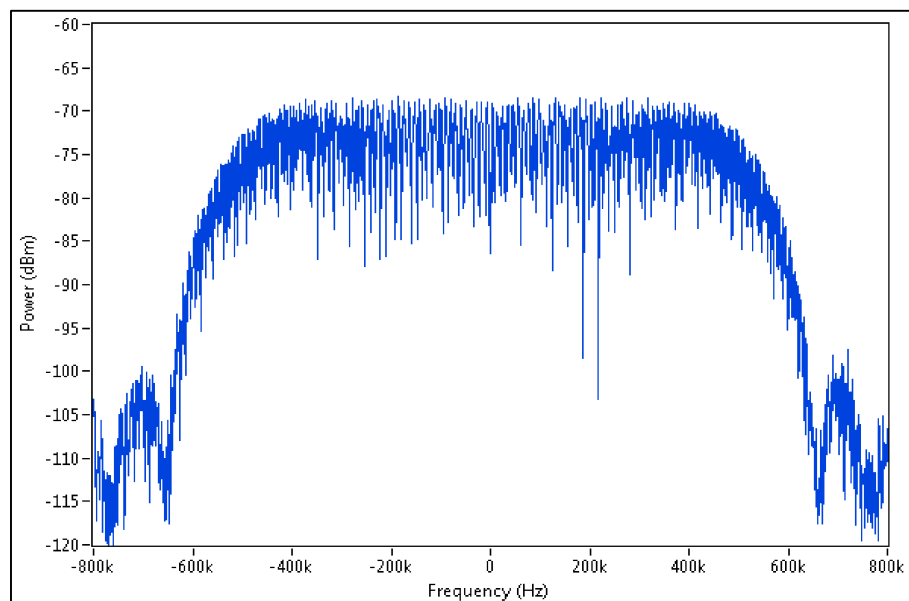


Figure 4.5. Received spectrum for 1 M sym/s for a 16 QAM signal with 100 ns delay spread and no Doppler shift.

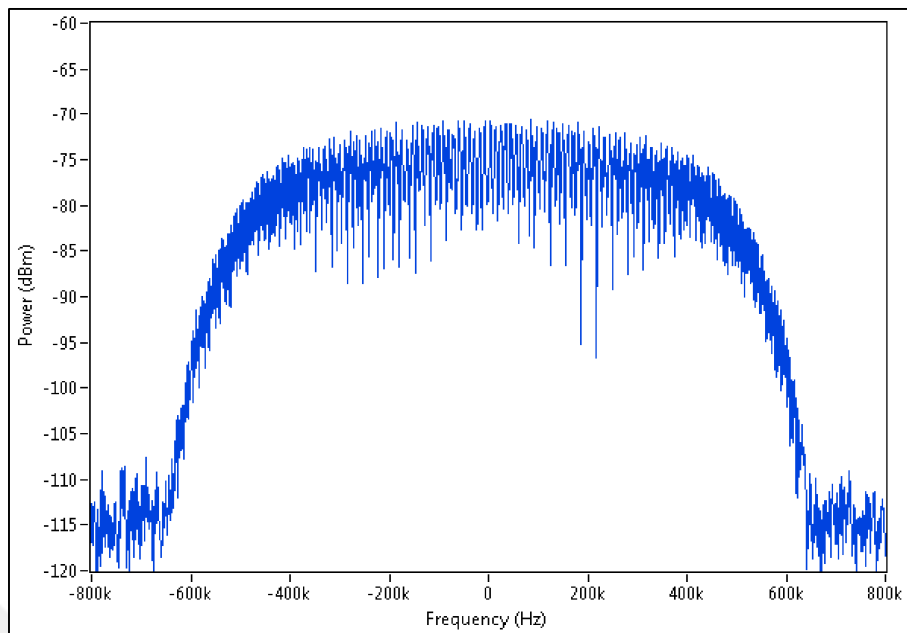


Figure 4.6. Received spectrum for 1 M sym/s for a 16 QAM signal with 1 us delay spread and no Doppler shift

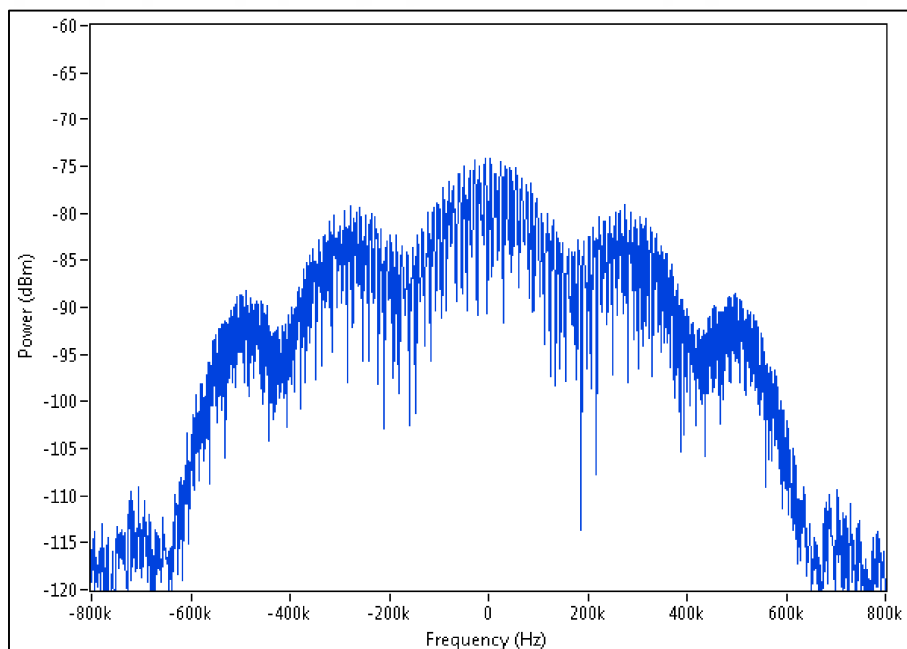


Figure 4.7. Received spectrum for 1 M sym/s for a 16 QAM signal with 4 us delay spread and no Doppler shift

4.2.2. Communication Performance

The purpose of this test is to verify that the communication performance decreases as the channel bandwidth gets narrower. In other words when the channel bandwidth is smaller than the signal bandwidth the communication performance gets degraded significantly. EVM and constellation diagrams for several cases are summarized in Table 4.1 and Figures 4.8, 4.9 and 4.10.

Table 4.1. EVM measurements for different delay spread values on a 1 M sym/s 16 QAM signal

Delay Spread (ns)	EVM
100	-42,5
1000	-23,2
4000	-2.6

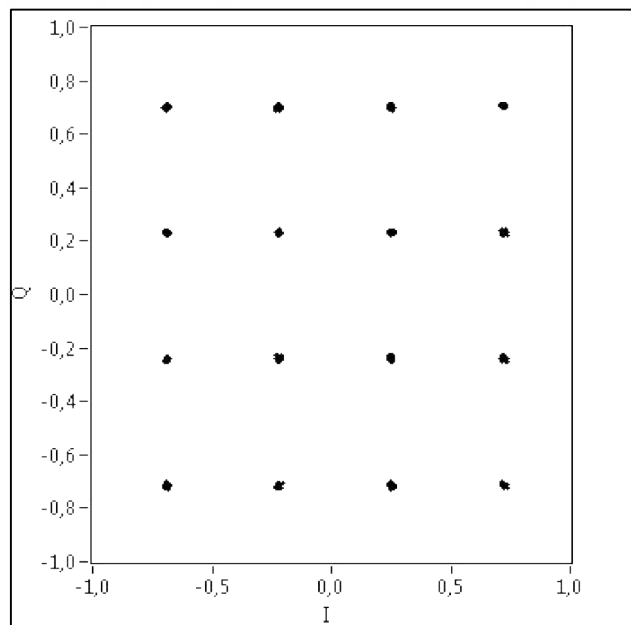


Figure 4.8. Constellation plot for 1 M sym/s for a 16 QAM signal with 100 ns delay spread and no Doppler shift.

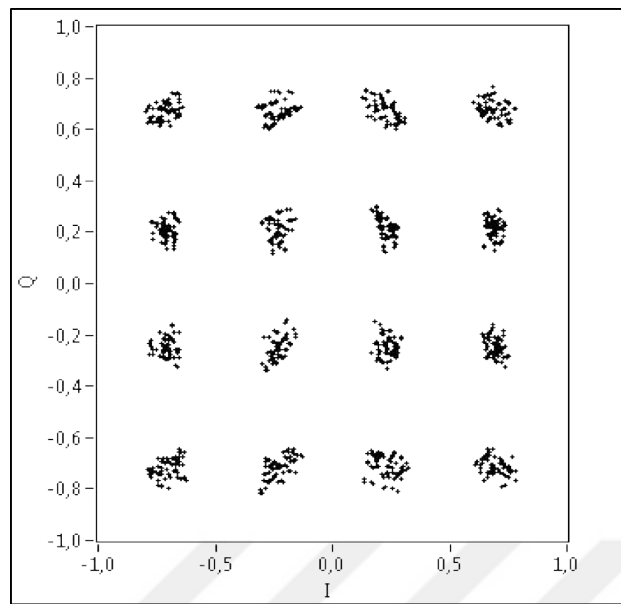


Figure 4.9. Constellation plot for 1 M sym/s for a 16 QAM signal with 1 us delay spread and no Doppler shift.

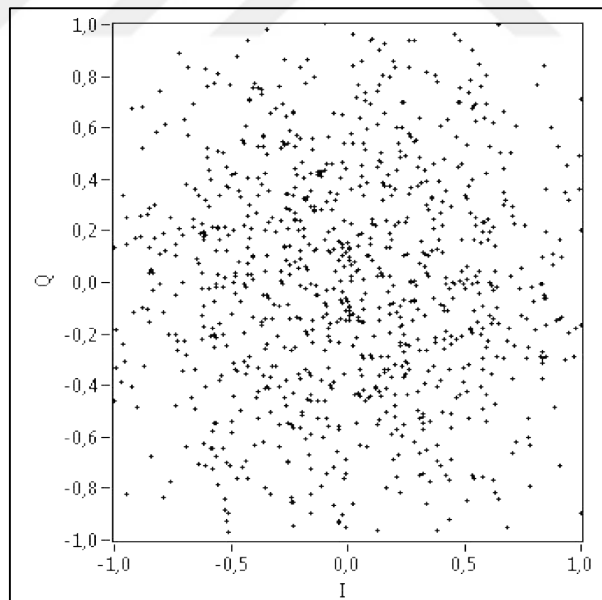


Figure 4.10. Constellation plot for 1 M sym/s for a 16 QAM signal with 4 us delay spread and no Doppler shift.

4.3. EFFECTS OF FREQUENCY DISPERSION

Effects of frequency dispersion have been investigated first on frequency domain in order to see the filter effect of the channel. After that, communication performance has been investigated with communication analysis tools.

4.3.1. Frequency Domain Analysis

Frequency dispersion is implemented using Jakes mobile fading. Although frequency dispersion is not observed significantly on spectral shape, the peak amplitude of the spectrum decreases after the dispersion algorithm as shown in Figures 4.11 and 4.12.

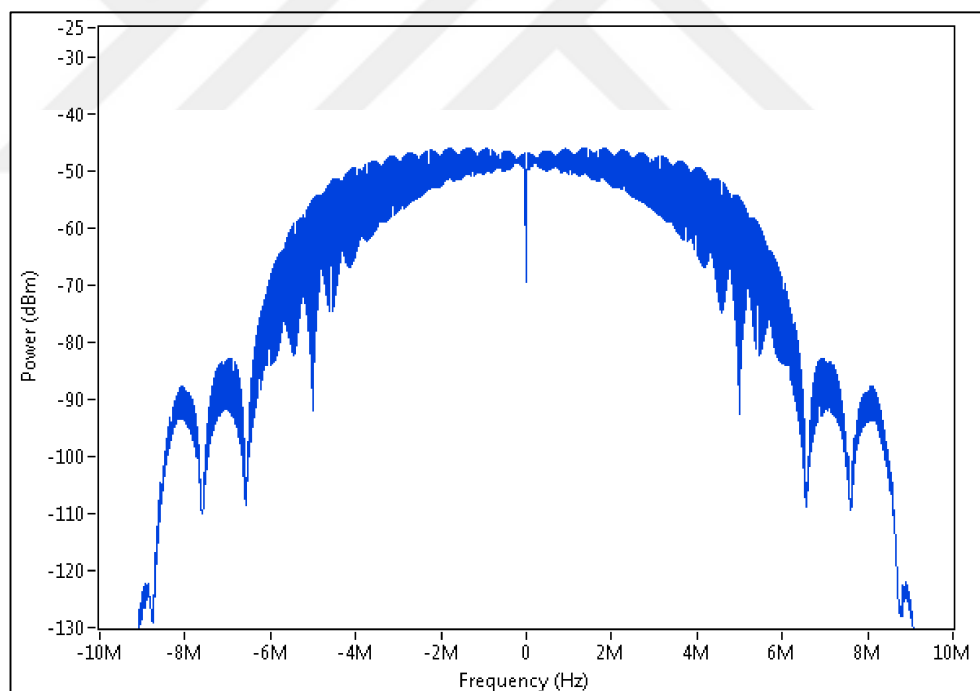


Figure 4.11. Received Spectrum for 10 M sym/s for a 4 QAM signal with 100 ns delay spread and no Doppler shift.

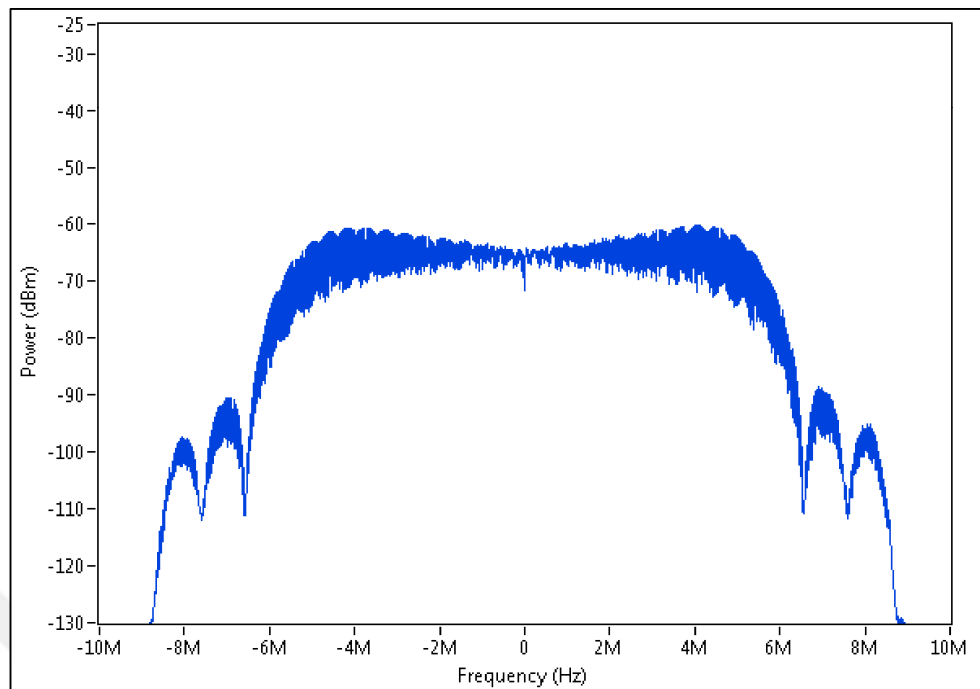


Figure 4.12. Received Spectrum for 10 M sym/s for a 4 QAM signal with 100 ns delay spread and 1000 Hz Doppler shift.

4.3.2. Communication Performance

Significant increase on Doppler spread adversely affects the communication quality as shown in Figures 4.13 and 4.14. However, when the symbol time is much smaller than the coherence time of the channel, communication performance is affected less as displayed in Figures 4.15 and 4.16. Figure 4.17 shows that modulations with low symbol rates are less resistant to frequency spread. Table 4.2 shows the EVM measurement versus Doppler spread for a 4-QAM signal with 1 M sym/s and Table 4.3 shows the EVM measurements versus baud rate for the same signal and for 100 Hz Doppler spread. It can be clearly observed that the relation between the coherence time and baud rate is a critical factor for digital communications.

Table 4.2. EVM measurements for different Doppler spread values on a 1 M sym/s 4QAM signal with 100ns delay spread.

Doppler Spread	EVM
100	-14,4
300	-6,98
1000	-1,45

Table 4.3. EVM measurements on a 4 QAM signal for 100Hz Doppler spread with 100ns delay spread.

Baud Rate	EVM
100 k	-7,1
1M	-14,4
10M	-21

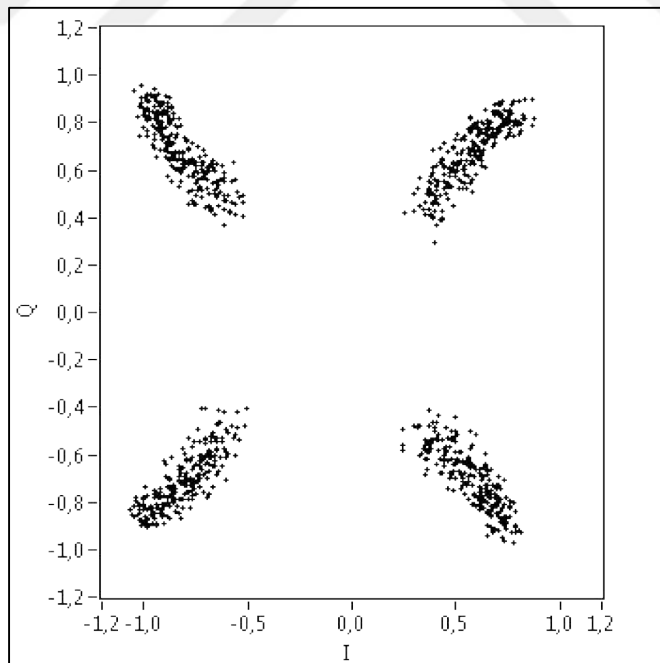


Figure 4.13. Constellation plot for 1 M sym/s for a 4 QAM signal with 100 ns delay spread and 100 Hz Doppler shift.

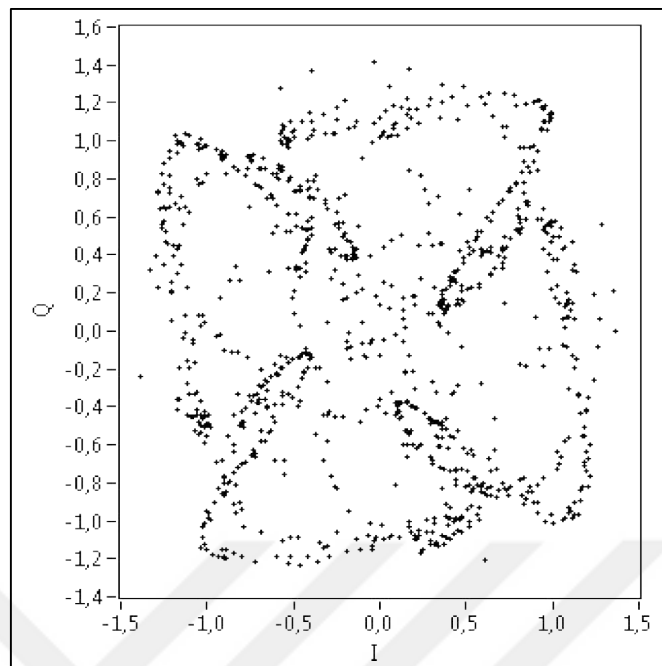


Figure 4.14. Constellation plot for 1 M sym/s for a 4 QAM signal with 100 ns delay spread and 1000 Hz Doppler shift.

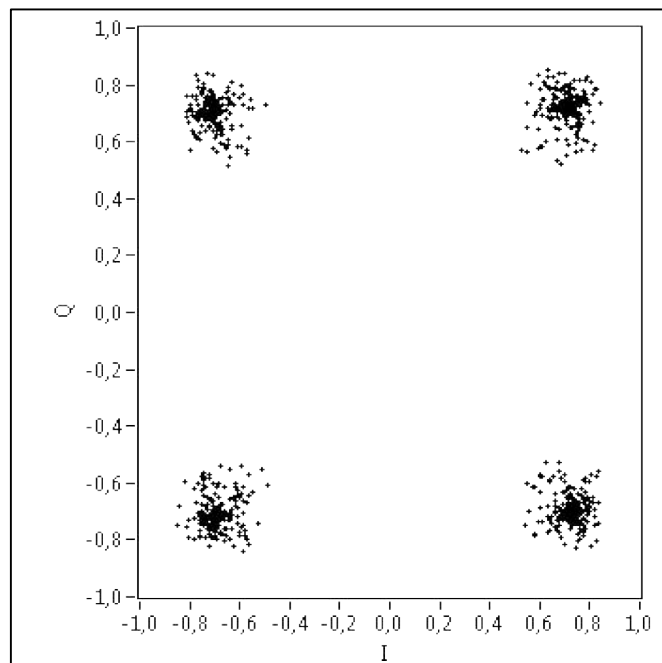


Figure 4.15. Constellation plot for 10 M sym/s for a 4 QAM signal with 100 ns delay spread and 100 Hz Doppler shift.

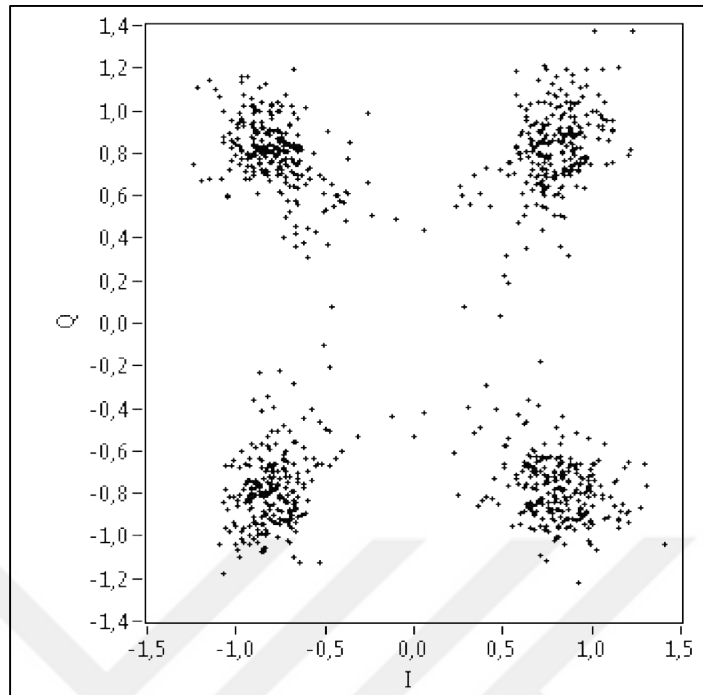


Figure 4.16. Constellation plot for 10 M sym/s for a 4 QAM signal with 100 ns delay spread and 1000 Hz Doppler shift.

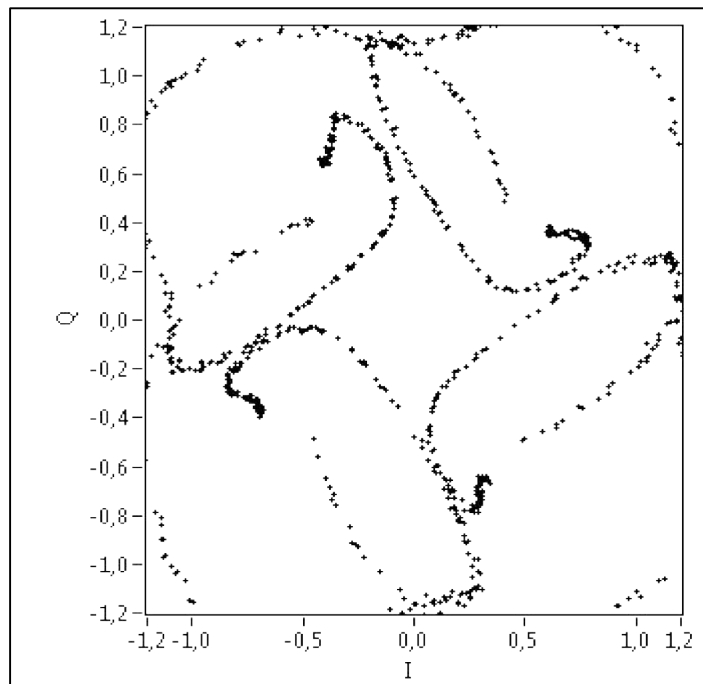


Figure 4.17. Constellation plot for 100 k sym/s for a 4 QAM signal with 100 ns delay spread and 100 Hz Doppler shift.

4.4. LTE PERFORMANCE

NI LTE Generation Toolkit is used to generate signals to test LTE signals that conform to the 3GPP specifications. Performance tests on LTE has been executed with an Uplink (FDD) signal with 10 MHz BW and with Quadrature Phase Shift Keying (QPSK) modulation and the results are shared in Figures 4.18, 4.19, 4.20, and Table 4.4.

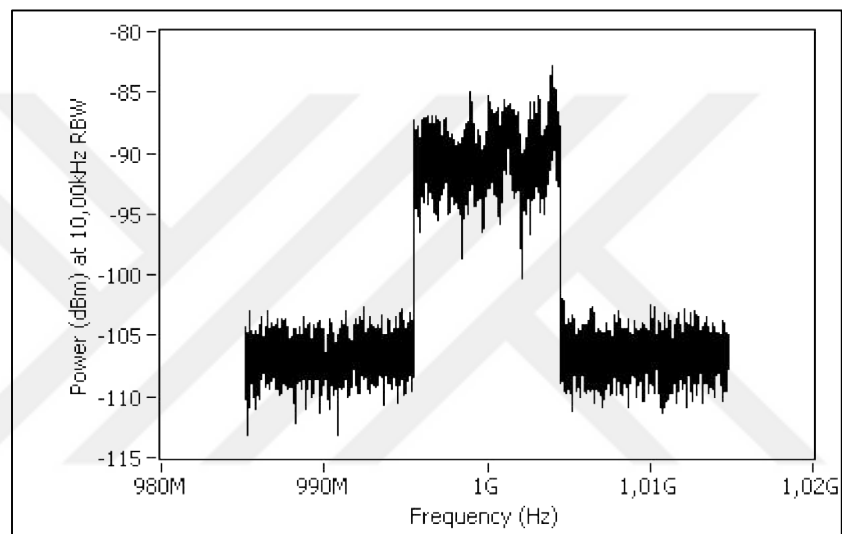


Figure 4.18. LTE spectrum for 1 us delay spread and 100 Hz Doppler shift.

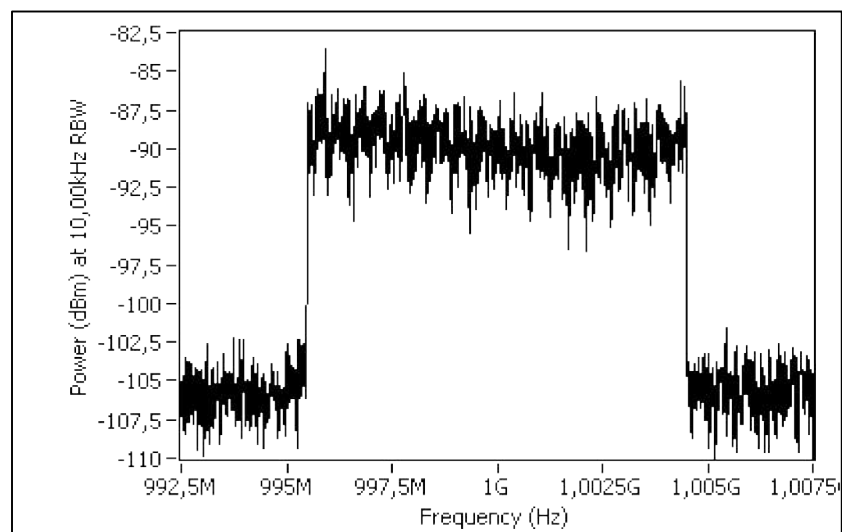


Figure 4.19. LTE spectrum for 100 ns delay spread and 300 Hz Doppler shift.

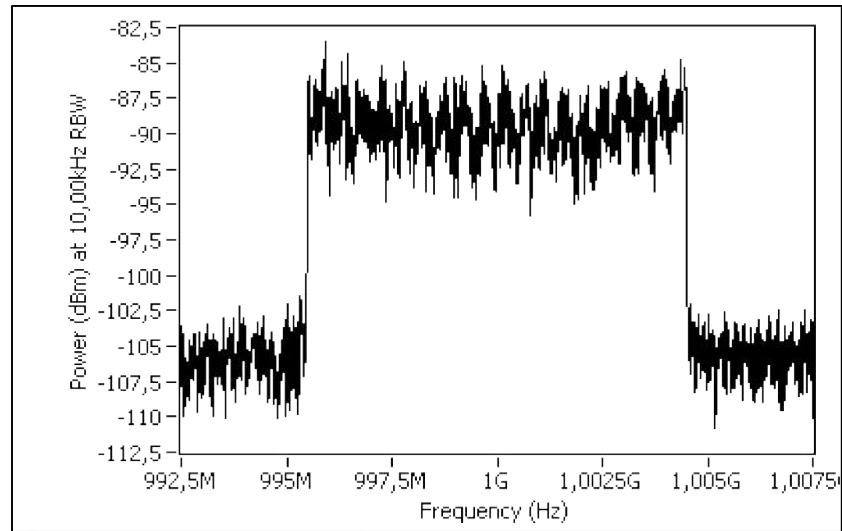


Figure 4.20. LTE spectrum for 100 ns delay spread and 1000 Hz Doppler shift.

Table 4. 4. EVM measurements for 100Hz Doppler spread with 100ns delay spread.

Delay Spread (ns)	Doppler Spread	PUSCH EVM	PUSCH DMRS EVM	PUSCH Data EVM
1000	100	NaN	NaN	NaN
100	300	-7,89	-12,18	-7,47
100	1000	-6,53	-10,29	-6,13

4.5. INTERFERENCE MEASUREMENTS

The first interference measurement has been done by generating a high power single tone signal that is 1.7 MHz away from the signal of interest which is 4 QAM signal with 1 M Sym/s symbol rate that passed from the propagation channel algorithm. Two signals have been added with an RF combiner. The spectrum is highly distorted on a very wide band as shown in Figure 4.21. The main reason of the distortion is the saturation of the RF mixer on the VSA and non-linear response of the amplifiers.

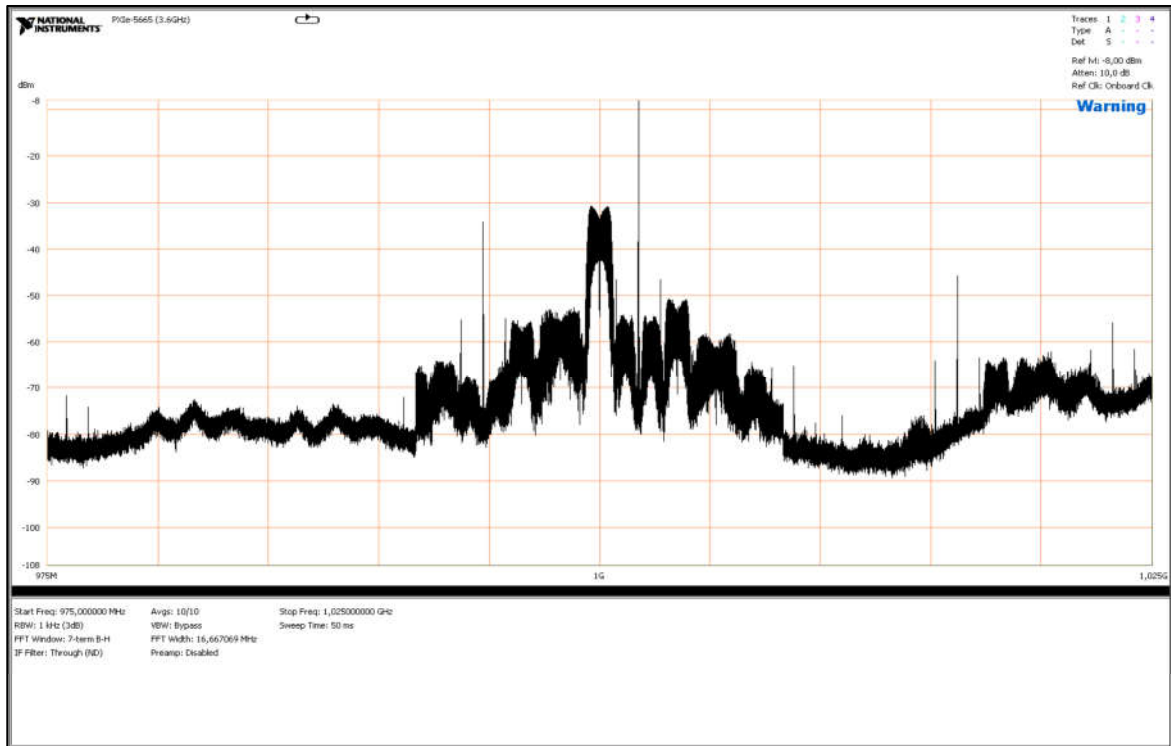


Figure 4.21. VSA spectrum screen for high power adjacent channel signal

In order to simulate the adjacent channel interference, an RF pulse has been generated at 5 MHz away from the 4 QAM signal. The pulse leaks in the adjacent band and distorts the sidelobes the QAM signal as can be seen in Figure 4.22. The pulse leaks also in to the band of interest such that it causes a noise effect as can be observed from Figure 4.23.

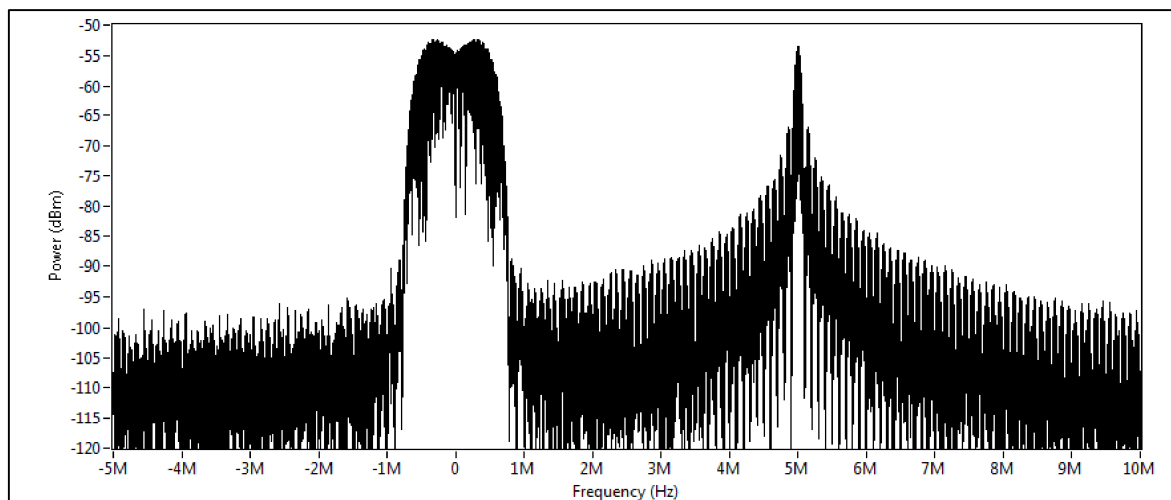


Figure 4.22. Received spectrum for a 4 QAM and an adjacent pulse

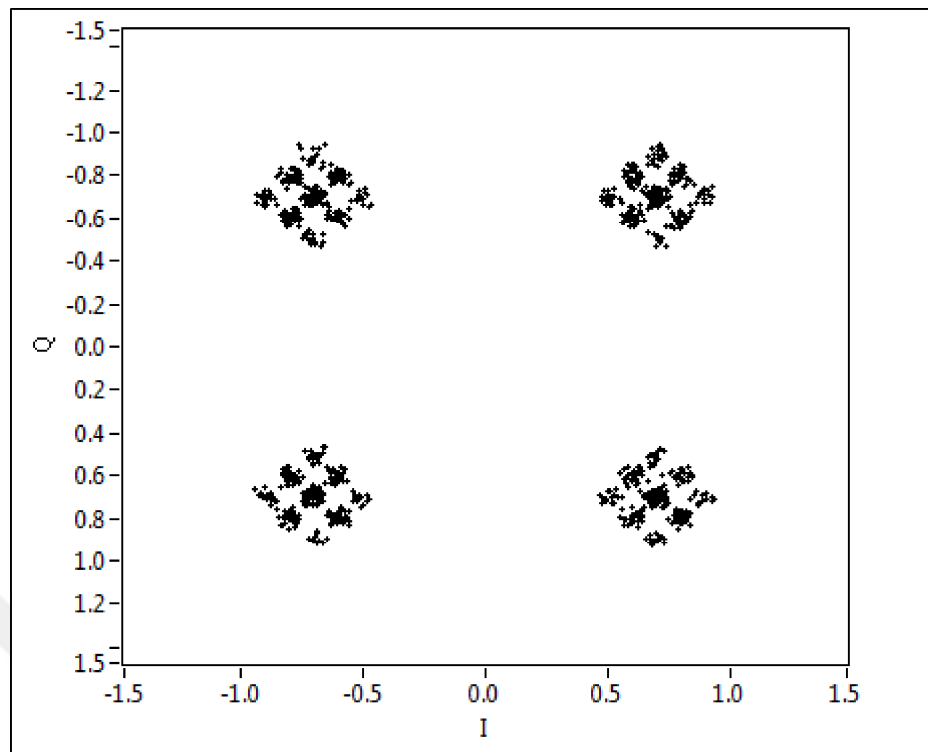


Figure 4.23. Received spectrum for 1 M sym/s for a 4 QAM signal in the presence of an adjacent pulse

The intermodulation distortions has been simulated via a nonlinear function and a lesser effect of the used RF hardware. An 8 PSK and a 16 QAM signal has been generated from the same RF output with frequency shifts as can be seen in Figure 4.24. The harmonics and intermodulation products can cause any type of interference for another signal of interest.

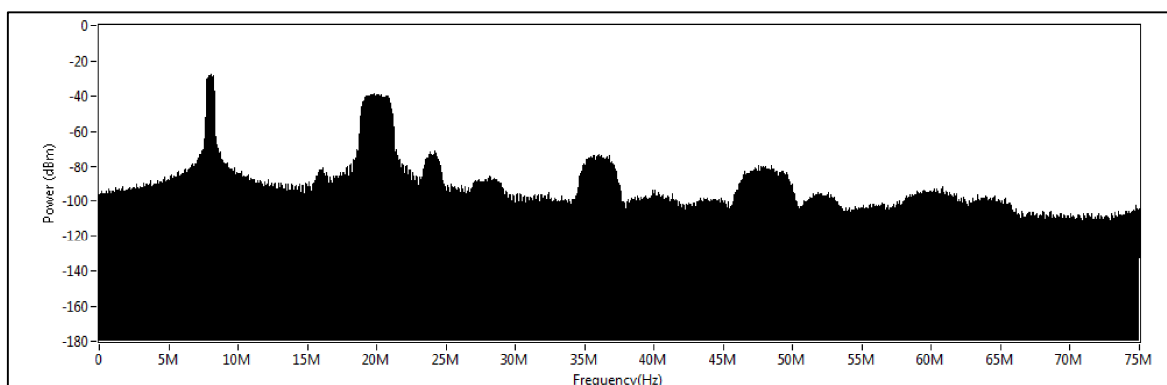


Figure 4.24. Output spectrum of the non linear function for and 8 PSK and a 16 QAM signal.

5. CONCLUSIONS

In this study, a generic, programmable RF Environment Simulation software has been implemented on NI VSG. Besides the statistical channel models, effects of the troposphere and the terrain have been included in the simulations. Utilization of real hardware enabled simulation results closer to real world ones. Multiple signals with different modulation structures can be generated and their interaction with each other and with the environment can be modeled. The novelty in the proposed architecture is that it enables arbitrary phase profiling in time and in frequency, and the hardware setup is built on software defined radio platform. The bandwidth of the system can be easily expanded using a higher rate ADC. In theory, the software can utilize arbitrary number of signals. Developed architecture is relatively cheap and easy to implement especially for radar studies.

In order to increase the simulation accuracy, antenna pattern can be included in the calculations or the system can be run with real antennas. Angle of arrival values for each path provided by a commercial ray propagation software such as Wireless In Site will increase the simulation accuracy when combined with the antenna pattern. The angle of arrival values can also be used to enhance Doppler spread calculations in future studies. Since it is possible to generate any type of signals with flexible parameters, it is also possible to use this system to generate the appropriate conditions for EMI and EMC test of devices. On the other hand, effect of the electromagnetic emissions caused by any device can be measured or monitored when the system is used with real antennas.

REFERENCES

1. William H. Tranter, K. Sam Shanmugan, Theodore S. Rappaport, Kurt L. Kosbar, Modeling and simulation of Waveform Channels, *Principles of Communication Systems Simulation with Wireless Application*, Upper Saddle River, New Jersey: Prentice Hall., 2003, pp. 536-572
2. Philip A. Bello, Characterization of Randomly Time-Variant Linear Channels, *IEEE Transactions on Communication Systems*, December 1963, p. 360–393.
3. F. Pe´rez Fonta´n, P. Marin˜o Espin˜eira, Multipath: Wideband Channel, In *Modeling the Wireless Propagation Channel*, United Kingdom: John Wiley & Sons Ltd., 2008, pp.165-184
4. Yong Soo Cho, Jaekwon Kim, Won Young Yang, Chung G. Kan, SISO Channel Models, In *Mimo-Ofdm Wireless Communications with Matlab*, Singapore: John Wiley & Sons (Asia) Pte Ltd., 2010, pp. 50-53
5. P. Dent, G. E. Bottomley, T. Croft Jakes Fading Model Revisited, *Electronics Letters*, Volume 29, Number 13, 24th June 1993 p. 1162-1163
6. Bernard Sklar. Statistical Models for Multipath Fading Channels, homepage, <http://www.ni.com/white-paper/14913/en/#top> [retrieved 21 August 2017].
7. MathWorks, “Fading Channels”, <https://www.mathworks.com/help/comm/ug/fading-channels.html> [retrieved 21 August 2017.]
8. IZT GmbH Germany, “COMINT Simulator”, <https://www.izt-labs.de/en/products/category/signal-generators/product/comint-simulator/> [retrieved 21 August 2017.]
9. Keysight, “Propsim Channel Emulation Solutions”, <http://www.keysight.com/en/pc-2697334/propsim-channel-emulation-solutions?cc=US&lc=eng> [retrieved 21 August 2017.]
10. Spirent, <https://www.spirent.com/Products/SR5500-Channel-Emulator> [retrieved 21 August 2017.]

11. T.S. Rappaport, *Wireless Communications: Principles and Practice*, 2nd ed. Singapore: Pearson Education, Inc., 2002
12. Hans J. Liebe, Modeling attenuation and phase of radio waves in air at frequencies below 1000GHz, *Radio Science*, Volume 16, Number 6, November-December 1981 p. 1183-1199.
13. John S. Seybold, *Introduction to RF Propagation*. Hoboken, New Jersey: John Wiley & Sons, Inc., 2005
14. Rep. ITU-R P. 676-11, Attenuation by atmospheric gases, September 2016.
15. Rep. ITU-R P.372-13, Radio Noise, September 2016.
16. Rep. ITU-R P. P.369-6, Reference Atmosphere For Refraction, August 1994.
17. A.G.Longley, P.L.Rice, Prediction of Tropospheric Radio Transmission Loss over Irregular Terrain, Institute for Telecommunication Services, Colorado, July 1968
18. Rep. ITU-R P. P.1546-4, Method for point-to-area predictions for terrestrial services in the frequency range 30 MHz to 3 000 MHz, October 2009.
19. Robert S. Mawrey, *Radio Frequency Interference and Antenna Sites*. Hoboken, New Jersey: John Wiley & Sons, Inc., 2005
20. Raymond McArthur. Intermodulation Fundamentals, homepage, [http://www.sinclairtechnologies.com/white_%20papers/Intermod\(2\).pdf](http://www.sinclairtechnologies.com/white_%20papers/Intermod(2).pdf) [retrieved 25 August 2017].
21. Cobham, “Intermodulation Distortion App Note” <http://ats.aeroflex.com/support/technical-support/product-support-documents/2026a-app-notes> [retrieved 25 August 2017].
22. Abhijit Mitra. *Lecture Notes on Mobile Communication*, Indian Institute of Technology Guwahati, India, 2009.
23. Remcom, <https://www.remcom.com/wireless-insite-em-propagation-software/> [retrieved 21 August 2017.]

24. Remcom, “Site-specific Radio Propagation Prediction Software REFERENCE MANUAL” <https://www.remcom.com/wireless-insite-em-propagation-software/> [retrieved 21 August 2017.]
25. Remcom, “Propagation Prediction over Colorado Plains” <https://www.remcom.com/examples/propagation-prediction-over-colorado-plains.html> [retrieved 21 August 2017.]



APPENDIX A: VERTICAL PLANE PROPAGATION MODEL

Wireless InSite's Vertical Plane propagation model uses the UTD wedge diffraction coefficients with the modifications for finite conductivity and for multiple diffractions given. The advantages of wedge diffraction over knife-edge diffraction models and semi-empirical models in propagation prediction have been addressed in several papers. The advantages include the capability to include reflections, to accurately model the actual terrain and to include effects of finite conductivity and surface roughness. The UTD based model can provide precise predictions for situations where the terrain profile is accurately known, especially for shorter paths, since its computations include the reflections and diffractions for the particular terrain profile being considered. In many cases it is possible to calculate the path loss and other propagation characteristics using only the features in the vertical plane containing the transmitter and receiver of interest. Wireless InSite automatically extracts the vertical planes from the three-dimensional terrain data. The calculations are performed for all active transmitter and receiver sets. Wireless InSite is more accurate than other models because it computes both amplitude and phase of the electric fields for all the paths from the transmitter to the receiver and sums the complex valued fields to determine the total electric field and other derived quantities. The paths can undergo a maximum of four diffractions and an arbitrary number of reflections. In order to validate InSite's ability to model propagation over irregular terrain, Vertical Plane results were compared to path gain measurements performed by the Institute for Telecommunication Sciences (ITS) in near Longmont , Colorado [25].